Development/Plasticity/Repair

Myelinogenic Plasticity of Oligodendrocyte Precursor Cells following Spinal Cord Contusion Injury

Peggy Assinck,[1,2] Greg J. Duncan,[1,3] Jason R. Plemel,[5] Michael J. Lee,[1] Jo A. Stratton,[5] Sohrab B. Manesh,[1,2] Jie Liu,[1] Leanne M. Ramer,[6] Shin H. Kang,[7] Dwight E. Bergles,[7] Jeff Biernaskie,[5,8,9] and Wolfram Tetzlaff[1,3,4]

[1]International Collaboration on Repair Discoveries, [2]Graduate Program in Neuroscience, [3]Department of Zoology, and [4]Department of Surgery, University of British Columbia, Vancouver, British Columbia V6T 1Z4, Canada, [5]Hotchkiss Brain Institute, University of Calgary, Calgary, Alberta T2N 1N4, Canada, [6]Department of Biomedical Physiology and Kinesiology, Simon Fraser University, Burnaby, British Columbia V6A 1N4, Canada, [7]Solomon H. Snyder Department of Neuroscience, Johns Hopkins University School of Medicine, Baltimore, Maryland 21205, and [8]Alberta Children's Hospital Research Institute and [9]Faculty of Veterinary Medicine, University of Calgary, Calgary, Alberta T2N 1N4, Canada

Spontaneous remyelination occurs after spinal cord injury (SCI), but the extent of myelin repair and identity of the cells responsible remain incompletely understood and contentious. We assessed the cellular origin of new myelin by fate mapping platelet-derived growth factor receptor α (PDGFRα), Olig2+, and P0+ cells following contusion SCI in mice. Oligodendrocyte precursor cells (OPCs; PDGFRα+) produced oligodendrocytes responsible for *de novo* ensheathment of ~30% of myelinated spinal axons at injury epicenter 3 months after SCI, demonstrating that these resident cells are a major contributor to oligodendrocyte regeneration. OPCs also produced the majority of myelinating Schwann cells in the injured spinal cord; invasion of peripheral myelinating (P0+) Schwann cells made only a limited contribution. These findings reveal that PDGFRα+ cells perform diverse roles in CNS repair, as multipotential progenitors that generate both classes of myelinating cells. This endogenous repair might be exploited as a therapeutic target for CNS trauma and disease.

Key words: myelin; NG2 glia; oligodendrocytes; OPCs; Schwann cells; spinal cord injury

Significance Statement

Spinal cord injury (SCI) leads to profound functional deficits, though substantial numbers of axons often survive. One possible explanation for these deficits is loss of myelin, creating conduction block at the site of injury. SCI leads to oligodendrocyte death and demyelination, and clinical trials have tested glial transplants to promote myelin repair. However, the degree and duration of myelin loss, and the extent and mechanisms of endogenous repair, have been contentious issues. Here, we use genetic fate mapping to demonstrate that spontaneous myelin repair by endogenous oligodendrocyte precursors is much more robust than previously recognized. These findings are relevant to many types of CNS pathology, raising the possibility that CNS precursors could be manipulated to repair myelin in lieu of glial transplantation.

Introduction

Spinal cord injury (SCI) causes both primary neural injury and secondary tissue damage (Kwon et al., 2002, 2004; Norenberg et al., 2004). Secondary injury leads to oligodendrocyte death and axon demyelination, which may leave axons vulnerable to degeneration (Bresnahan et al., 1976; Blight, 1983; Crowe et al., 1997; Totoiu and Keirstead, 2005; McTigue and Tripathi, 2008; Plemel et al., 2014). Remyelination of axons in and around the SCI site is viewed as an important element of regeneration (R. P. Bunge et

Received July 28, 2016; revised June 22, 2017; accepted July 22, 2017.

Author contributions: P.A., G.J.D., J.R.P., L.M.R., J.B., and W.T. designed research; P.A., G.J.D., J.S.S., and J.L. performed research; S.H.K., D.E.B., J.B., and W.T. contributed unpublished reagents/analytic tools; P.A., M.J.L., and S.B.M. analyzed data; P.A., G.J.D., J.R.P., L.M.R., D.E.B., J.B., and W.T. wrote the paper.

This work was supported by the Canadian Institutes for Health Research (CIHR; MOP-130475), the Craig H. Neilsen Foundation (D.E.B.), and the National Institutes of Health (NIH NS051509); a Frederick Banting and Charles Best Canadian Graduate Scholarship-Doctoral Award to P.A.; a Multiple Sclerosis Society of Canada Doctoral Scholarship to G.J.D.; the Donna Joan Oxford Postdoctoral Fellowship Award from the Multiple Sclerosis Society of Canada and postdoctoral fellowship awards from CIHR, T. Chen Fong, and Alberta Initiatives Health Solutions to J.R.P. We thank Dr. William Richardson (University College London, London) for the *PDGFRα-CreER^{T2}(II)* mice, Dr. Hiroshi Takebayashi via the laboratory of Dr. Scott Whittemore (Louisville, KY) for the *Olig-2creER^{TM}* mice, and Dr. Ueli Suter (ETH, Zürich) for the *P0-CreER^{T2}* mice; Drs. Brett J. Hilton and Joseph Sparling, for valuable intellectual inputs; Yuan Jiang, Jasdeep Grewal, Danielle Chan, and Daniel Sykora for their technical assistance; Nathan Michaels for assistance with breeding and husbandry; and Dr. Michael Wegner for his gift of the MYRF antibody.

The authors declare no competing financial interests.

Correspondence should be addressed to Dr. Wolfram Tetzlaff, University of British Columbia, Blusson Spinal Cord Centre, 818 West 10th Avenue, Vancouver, BC, V5Z 1M9 Canada. E-mail: tetzlaff@icord.org.

S. H. Kang's present address: Shriners Hospitals Pediatric Research Center, Temple University Lewis Kratz School of Medicine, Philadelphia, PA 19140.

DOI:10.1523/JNEUROSCI.2409-16.2017

 0270-6474/17/378635-20$15.00/0

al., 1960; Totoiu and Keirstead, 2005; Almad et al., 2011; James et al., 2011; Powers et al., 2012; Plemel et al., 2014) and has provided a rationale for clinical trials involving transplantation of neural precursor cells (Cummings et al., 2005; Keirstead et al., 2005; Priest et al., 2015). To avoid the costs and safety concerns of transplantation, an alternative strategy may be to augment spontaneous remyelination after SCI (Assinck et al., 2017). However, it is critical to determine the contributions of various endogenous progenitors to this regenerative process (Barnabé-Heider et al., 2010; Grégoire et al., 2015; Stenudd et al., 2015).

The extent of oligodendrocyte remyelination following SCI has been quantified using indirect measures, based on the assumption that new myelin sheaths are thinner (Blakemore, 1974). However, using internodal length to identify new myelin sheaths and axonal tracing to identify a specific tract after SCI, it was discovered that new myelin is only marginally thinner after SCI in rodents (Lasiene et al., 2008; Powers et al., 2012, 2013). Evaluating the extent of spontaneous remyelination based on thin myelin likely represents a considerable underestimation of repair; thus, the true extent of spontaneous oligodendrocyte myelination following SCI remains unknown.

Myelinating oligodendrocytes are derived from oligodendrocyte precursor cells (OPCs), characterized by the expression of NG2 and platelet-derived growth factor receptor α (PDGFRα) (Nishiyama et al., 1996; Rivers et al., 2008; Kang et al., 2010; Young et al., 2013). Mice expressing inducible Cre recombinase (CreER) under control of PDGFRα promoter/enhancers allow *in vivo* tracking of oligodendrocyte lineage cells (Rivers et al., 2008; Kang et al., 2010) and reveal that PDGFRα-expressing cells generate new myelinating oligodendrocytes as late as 3 months after SCI (Hesp et al., 2015). Given the persistence of OPC differentiation, it is particularly important to determine the magnitude of their contribution to remyelination after SCI.

In addition to oligodendrocytes, Schwann cells contribute to the myelination of axons after CNS damage, both in SCI (Bresnahan, 1978; R. P. Bunge et al., 1993; Guest et al., 2005) and in demyelinating lesions of the spinal cord (Blakemore, 1975). In these settings, Schwann cell myelination of spinal axons is predominately localized to areas of significant astrocyte loss (Itoyama et al., 1985). The prevailing view has been that Schwann cells migrate into the damaged spinal cord from the peripheral nervous system (PNS) via spinal nerve roots, meningeal fibers, or autonomic nerves following breakdown of the glia limitans (Franklin and Blakemore, 1993). However, PDGFRα+ cells also give rise to Schwann cells following demyelinating chemical lesions (Zawadzka et al., 2010). The contribution of OPCs to oligodendrocyte and Schwann cell myelination after a clinically relevant contusion SCI has not been determined using *in vivo* fate mapping techniques.

Here, we systematically assessed the capacity of multiple cell types to form myelinating oligodendrocytes and Schwann cells following contusion SCI. We demonstrate that PDGFRα+ OPCs contribute to ~30% of myelin sheaths surrounding axons in the vicinity of the lesion site 12 weeks after injury. We further show that PDGFRα^+ OPCs give rise to the majority of myelinating Schwann cells found in the spinal cord after injury, with only a small contribution stemming from the P0+ peripheral Schwann cell population. These data reveal the diverse behavior of endogenous PDGFRα+ cells in response to SCI and reveal that they contribute substantially to myelin regeneration.

Materials and Methods

Transgenic mice and Cre induction

Two lines of *PDGFRα-CreER^{T2}* mice, *PDGFRα-CreER* (I; Kang et al., 2010; Jackson Laboratories, RRID: IMSR_JAX:018280) and *PDGFRα-CreER^{T2}*(II; Rivers et al., 2008), were crossed with *Rosa26-eYFP* (Jackson Laboratories, RRID: ISMR_JAX:006148) or the membrane-tethered *Rosa26-mGFP(mT/mG)* (Jackson Laboratories, RRID: ISMR_JAX:007576) reporter mice. In addition, *Olig2-CreER* (Takebayashi et al., 2002) and *P0-CreER^{T2}* (Leone et al., 2003) mouse lines were individually crossed with the *Rosa26-eYFP* reporter mouse. PDGFRα+ cells for *in vitro* experiments were isolated from *PDGFRα:H2B-GFP* mice (Hamilton et al., 2003; Jackson Laboratories, RRID: ISMR_JAX:007669) via flow cytometry (FACS). An overview of the transgenic mice used is provided in Tables 1 and 2.

All experiments were performed in accordance with protocols approved by the University of British Columbia and University of Calgary animal care committees and the Canadian Council on Animal Care. Mice of either sex were group housed (2–6 mice/cage, genders separated) in secure conventional rodent facilities on a 12 h light/dark cycle with constant access to food and water. Cre-mediated recombination was induced at 8–10 weeks of age via intraperitoneal tamoxifen (Sigma-Aldrich, T5648) dissolved in corn oil at 20 mg/ml. *PDGFRα-CreER(I):Rosa26-eYFP*, *PDGFRα-CreER(I):Rosa26-mGFP(mT/mG)*, *PDGFRα-CreER^{T2}(II):Rosa26-eYFP*, *Olig2-CreER:Rosa26-eYFP*, and *P0-CreER^{T2}:Rosa26-eYFP* mice received 3 mg of tamoxifen per day for 5 consecutive days; *PDGFRα-CreER^{T2}(II):Rosa26-mGFP(mT/mG)* received 0.5 mg of tamoxifen for 2 consecutive days. Tamoxifen-free controls (corn oil only injections) were included in all mouse lines both in injured and noninjured mice.

Surgical procedures

After the final day of tamoxifen injection, we allowed 2 weeks for tamoxifen clearance before mice received a SCI. One and 2 week clearances in the *PDGFRα-CreER (I):Rosa26e-YFP* mice were tested; results were qualitatively similar for both clearing intervals. All spinal cord, dorsal root, and sciatic nerve injuries, as well as the harvesting of dorsal roots and sciatic nerves from the *PDGFRα:H2B-GFP* mice, were performed at 10–12 weeks of age.

Spinal cord injury. Thoracic contusion SCI was delivered with the Infinite Horizons Impactor (Precision Systems Instrumentations). Animals were anesthetized using isofluorane (4% induction, 1.5% maintenance) and received buprenorphine (Temgesic; 0.02 mg/kg, s.c., McGill University) preoperatively. After the skin at the surgical site was shaved, cleaned, and disinfected, the animal was secured in a stereotaxic frame on a warming blanket; body temperature was maintained at 36.5°C. The spine was exposed via a midline incision in the skin and superficial muscles, and blunt dissection of the muscles over the T8–T11 vertebrae. The spinal cord was exposed via a T9–T10 laminectomy and the vertebrae were stabilized with clamps. The impactor delivered a 70 kdyne midline contusion injury. After injury, the muscle and skin were closed with continuous 5-0 Vicryl sutures, and interrupted 4-0 Prolene sutures, respectively. Animals received buprenorphine and lactated Ringer's (1 ml, s.c.) every 12 h for 48 h following SCI. Bladders were expressed twice daily until spontaneous micturition returned (~1–2 weeks after SCI). A subset of animals, received 5-ethynyl-2′-deoxyuridine (EdU;) for the first 2 weeks following SCI. Injured mice were killed and transcardially perfused at 1, 3, and 12 weeks post-injury (wpi). In addition, "uninjured controls" were perfused 2 weeks post-tamoxifen when the injury would have been sustained and "uninjured age-matched controls" were perfused alongside the 12 wpi group to assess cell formation at these time points in the absence of injury.

Root and nerve injury. We performed a dorsal root crush or a sciatic nerve crush in *PDGFRα-CreER(I):Rosa26-mGFP(mT/mG)* mice. As for SCI, animals were anesthetized using isofluorane and received buprenorphine preoperatively. The skin at the surgical site was shaved, cleaned, and disinfected. For sciatic nerve crush injury, a small proximal-to-distal incision was made in the skin immediately posterior to the left femur. The sciatic nerve was exposed and crushed twice 3 mm distal to the obturator tendon for 15 s with no. 5 fine Dumont forceps. Similarly, for

Table 1. Overview of transgenic mouse lines

Transgenic mice	Labelled cell populations	Cellular label	Tamoxifen	Reference
PDGFRαCreER^{TM}(I): Rosa26eYFP	PDGFRα+ cells before injury:	Cytoplasmic YFP	3 mg/d	Kang et al., 2010;
	OPCs		for 5 d	Jackson Laboratories, 006148
Short form: *PDGFRαCreER(I): YFP*	Vascular-associated cells	Short form: YFP		
	Central canal-associated cells			
	PNS endoneurial cells (fibroblast-like)			
PDGFRαCreER^{TM}(I): Rosa26mGFP(mT/mG)	PDGFRα+ cells before injury:	Membrane-tethered	3 mg/d	Kang et al., 2010;
	OPCs	GFP	for 5 d	Jackson Laboratories, 007576
Short form: *PDGFRαCreER(I): mGFP*	Vascular-associated cells	Short form: mGFP		
	Central canal-associated cells			
	PNS endoneurial cells (fibroblast-like)			
PDGFRαCreER^{T2}(II): Rosa26eYFP	PDGFRα+ cells before injury:	Cytoplasmic YFP	3 mg/d	Rivers et al., 2008;
	OPCs		for 5 d	Jackson Laboratories, 006148
Short form: *PDGFRαCreER(II): YFP*	Vascular-associated cells	Short form: YFP		
	Central canal-associated cells			
	PNS endoneurial cells (fibroblast-like)			
PDGFRαCreER^{T2}(II): Rosa26mGFP(mT/mG)	PDGFRα+ cells before injury:	Membrane-tethered	0.5 mg/d	Rivers et al., 2008;
	OPCs	GFP	for 2 d	Jackson Laboratories, 007576
Short form: *PDGFRαCreER(II): mGFP*	Vascular-associated cell	Short form: mGFP		
	Central canal-associated cells			
	PNS endoneurial cells (fibroblast-like)			
Olig2CreER^{TM}: Rosa26eYFP	Olig2 + cells before injury:	Cytoplasmic YFP	3 mg/d	Takebayashi et al., 2002;
	OPCs		for 5 d	Jackson Laboratories, 006148
Short form: *Olig2CreER: YFP*	Oligodendrocytes	Short form: YFP		
	Population of grey matter astrocytes			
P0CreER^{T2}: Rosa26eYFP	P0 + cells before injury:	Cytoplasmic YFP	3 mg/d	Leone et al., 2003;
Short form: *P0CreER: YFP*	Myelinating peripheral Schwann cells	Short form: YFP	for 5 d	Jackson Laboratories, 006148
PDGFRα:H2B-GFP	Cells currently expressing PDGFRα:	Cytoplasmic YFP	n/a	Hamilton et al., 2003;
	PDGFRα+ cells in CNS and PNS	Short form: YFP		Jackson Laboratories, 007669

dorsal root crush injury, the left C5 and C6 roots were exposed via a lateral hemilaminectomy and durotomy, and crushed twice for 15 s. Mice were perfused 2 weeks post-tamoxifen and termed uninjured controls and injured mice were perfused at either 4 or 12 wpi.

Tissue preparation and immunohistochemistry

Mice were deeply anesthetized and transcardially perfused with PBS followed by cold 4% paraformaldehyde. The spinal cord, dorsal root, and sciatic nerves were harvested and postfixed in 4% paraformaldehyde (2 h postfixation for dorsal and sciatic nerves; 6 h for spinal cord) before cryoprotection in a series of increasingly concentrated sucrose solutions. Tissue was frozen in OCT Embedding Compound (Tissue-Tek, Electron Microscopy Sciences), sectioned in either the longitudinal or cross-sectional plane (as stated in figure legends) at 20 μm thickness on a cryostat, and stored at −80°C. Before immunohistochemistry, frozen sections were thawed, then rehydrated in PBS, and incubated in 10% donkey serum dissolved in PBS with 0.1% Triton. Before immunohistochemistry targeting myelin, delipidization was performed using ascending and descending ethanol washes. Primary antibodies (Table 3) were applied overnight at room temperature, followed by application of the appropriate DyLight or AlexaFluor secondary antibodies (Jackson ImmunoResearch) for 2 h. In some sections, nuclei were labeled with Hoechst 33342 (RRID: AB_2651135; 1:1500). To visualize EdU, the Click-iT EdU AlexaFluor 647 (Invitrogen, C10340) Imaging Kit was used according to the manufacturer's instructions.

FACS and immunocytochemistry

Sciatic nerve segments (5 mm distal to the sciatic notch) and dorsal root/dorsal root ganglia (DRG; distal to dorsal root entry) were harvested from *PDGFRα:H2B-GFP* mice (4 independent experiments with 2–5 mice pooled per experiment) at 10–12 weeks of age. Tissue was finely chopped then incubated at 37°C for 30 min in collagenase Type-IV (Sigma-Aldrich, 1 mg/ml) followed by trituration (4× every 10 min) until a single cell suspension was obtained. Cells were resuspended in 0.1% bovine serum albumin (BSA)/HBSS and passed through a 40 μm filter, and GFP+ and GFP^{NEG} cells were sorted using FACS (BD Biosciences FACS Aria III, pressure 20 PSI, nozzle 100 μm). Sorted cells were collected and expanded for 1–2 weeks on coated poly-D-lysine/laminin (20 μg/ml) plates/slides, in Schwann cell proliferation/ differentiation media [1% horse serum, 1% penicillin/streptomycin, 2% N_2, bovine pituitary extract (20 ng/ml), neuregulin (10 ng/ml), forskolin (5 mM), L-glutamine in DMEM/F12]. For immunocytochemistry, cells were fixed in 2% paraformaldehyde for 5 min, then incubated with 0.5% TritonX and 5% BSA for 1 h. Primary antibodies (Table 3) were applied overnight at 4°C, and appropriate AlexaFluor secondary antibodies (Jackson ImmunoResearch) were applied for 2 h at room temperature followed by Hoechst stain (1:2000, 5 min). Images were captured on an Axio Observer inverted light microscope (Zeiss) or an Observer Fluorescence microscope (40× objective; Zeiss).

Cell counting and analysis

For assessing recombination efficiency in OPCs in the uninjured spinal cord, the *PDGFRα-CreER(I):Rosa26-eYFP* and *PDGFRαCreER^{T2}(II): Rosa26mGFP(mT/mG)* T9/10 mouse spinal cord sections at time of injury were processed immunohistochemically for GFP, PDGFRα, and Olig2 ($n = 3$ mice/group). Recombination efficiency percentages were reported as follows [% = (no. of nonvascular associated GFP+ PDGFRα+ Olig2+/no. of nonvascular associated PDGFRα+ Olig2+) × 100]. An average of 150 cells was counted per mouse.

For assessing oligodendrocyte lineage cell counts in *PDGFRα-CreER(I): Rosa26-eYFP* mice, we investigated either uninjured mice (uninjured 12 wpi age-matched control; $n = 3$) or mice post-SCI (3 wpi, $n = 4$; 12 wpi, $n = 6$) using sections stained for Olig2 (nuclear marker specific to the oligodendrocyte lineage), PDGFRα (OPCs), CC1 (oligodendrocytes), and YFP (recombined cells). A blinded observer determined the lesion epicenter by selecting the section with the least spared tissue based on axonal staining on another slide. Systematic random sampling was conducted in a single section (20×) at the epicenter or an equivalent T9/10 section for uninjured 12 wpi age-matched controls. This systematic random sampling included placing a large grid over the entirety of the cross-section at injury epicenter and randomly selecting a coordinate in each 3 × 3 subgridded area and imaging all the appropriate boxes within these coordinates. Boxes were equally spaced

Table 2. Overview of specific animal numbers that underwent quantitative or qualitative analysis

Group	Qualitative analysis	Quantitative analysis
PDGFRαCreER^{TM}(I): Rosa26eYFP		
Time of injury (uninjured spinal cord)	6	3
3 wpi (injured spinal cord)	10	7
12 wpi (injured spinal cord)	10	7
Week 12 uninjured (uninjured spinal cord)	6	4
Time of injury (uninjured sciatic nerve)	3	
No TA controls (injured spinal cord)	3	
No TA controls (uninjured spinal cord)	3	
PDGFRαCreER^{TM}(I): Rosa26mGFP(mT/mG)		
Time of injury (uninjured spinal cord)	3	
3 wpi (injured spinal cord)	3	
12 wpi (injured spinal cord)	10	
Week 12 uninjured (uninjured spinal cord)	6	
Time of injury (uninjured sciatic nerve)	3	
4 wpi (injured sciatic nerve)	3	
12 wpi (injured sciatic nerve)	3	
4 wpi (injured dorsal root	3	
12 wpi (injured dorsal root)	6	
No TA controls (injured spinal cord)	2	
No TA controls (uninjured spinal cord)	2	
PDGFRαCreER^{T2}(II): Rosa26eYFP		
12 wpi (injured spinal cord)	6	
Week 12 uninjured (uninjured spinal cord)	6	
No TA controls (injured spinal cord)	2	
No TA controls (uninjured spinal cord)	2	
PDGFRαCreER^{T2}(II): Rosa26mGFP(mT/mG)		
Time of injury (uninjured spinal cord)	6	3
3 wpi (injured spinal cord)	6	4
12 wpi (injured spinal cord)	6	5
Week 12 uninjured (uninjured spinal cord)	6	3
No TA controls (injured spinal cord)	2	
No TA controls (uninjured spinal cord)	2	
Olig2CreER^{TM}: Rosa26eYFP		
Time of injury (uninjured spinal cord)	3	
12 wpi (injured spinal cord)	10	
Week 12 uninjured (uninjured spinal cord)	6	
No TA controls (injured spinal cord)	4	
No TA controls (uninjured spinal cord)	4	
P0CreER^{T2}: Rosa26eYFP		
Time of injury (uninjured spinal cord)	6	
1 wpi (injured spinal cord)	6	5
3 wpi (injured spinal cord)	6	6
12 wpi (injured spinal cord)	10	7
Week 12 uninjured (uninjured spinal cord)	6	4
Time of injury (uninjured sciatic nerve)	3	
No TA controls (injured spinal cord)	2	
No TA Controls (uninjured spinal cord)	2	

See Materials and Methods for specific animal numbers for each analysis.

apart with 400 μm between boxes in any direction to ensure adequate sampling. Counts were conducted within optical dissector boxes with an area of 20,000 μm^2 each and cells were required to be Olig2+ to be included in the analysis. We then went on to count the number of Olig2+ cells that were PDGFRα+, CC1+, and/or YFP+. Percentages were calculated by taking the density of the cell of interest and dividing it by the density of the total population.

For examining oligodendrocyte ensheathment/myelination in *PDGFRα-CreER^{T2}(II): Rosa26-mGFP(mT/mG)* mice, we investigated either uninjured mice (uninjured 12 wpi age-matched control; $n = 3$) or mice post-SCI (3 wpi, $n = 4$; 12 wpi, $n = 5$) using sections stained for β3-tubulin, NF-200, and SMI312 collectively (to visualize axons), MBP (myelin), P0 (specific to peripheral myelin), and GFP (recombined cells). A blinded rater determined the lesion epicenter as described for assessing oligodendrocyte lineage cell counts. High-power (63× primary magnification) systematic random sampling was conducted in a single section at the epicenter or an equivalent T9/10 section for uninjured 12 wpi age-matched controls. This systematic random sampling (as described for oligodendrocyte lineage counts) used optical dissector boxes equally spaced apart (in the *x–y* plane) with a distance of 230 μm between boxes in any direction to ensure adequate sampling. The number of MBP+ axons were counted and then of those axons, the proportion of GFP+/^{NEG} sheaths around axons were counted. Additionally, we counted axons that were surrounded by GFP but were MBP^{NEG}. All counts were conducted within optical dissector boxes with an area of 400 μm^2 each and extrapolated to the entire cross section of the cord. Ensheathed/myelinated axons were only counted when a mGFP+ tube (new ensheathment/myelin) or MBP+ tube (myelin marker) entirely surrounded an axon profile (collectively: β3-tubulin+, NF-200+, and SMI312+). Total MBP+P0^{NEG} axons at epicenter were counted. Percentages of new mGFP+MBP+ axons at epicenter were calculated as follows: (mGFP+MBP+P0^{NEG}/MBP+P0^{NEG}) × 100. We then calculated the number of GFP+ tubes surrounding axons (split into the MBP+ or MBP^{NEG} ratios) as follows: (GFP+MBP+P0^{NEG}) + (GFP+MBP^{NEG}P0^{NEG}).

To examine the contribution of PDGFRα+ cells to Schwann cell remyelination after SCI, spinal cord sections from *PDGFRα-CreER(I): Rosa26-eYFP* were processed immunohistochemically for β3-tubulin, NF-200, and SMI312 collectively (to visualize axons), P0 (peripheral myelin), and YFP (recombined cells). High-power (63× primary magnification) cross-sectional images at lesion epicenter (as defined for examining oligodendrocyte ensheathment/myelination counts) were captured (week 12 uninjured, $n = 4$; 3 wpi, $n = 7$; 12 wpi, $n = 7$), and P0+/YFP+/^{NEG} myelin sheaths were counted.

To examine the contribution of P0+ cells to Schwann cell remyelination after SCI, spinal cord sections from *P0-CreER^{T2}:Rosa26-eYFP* mice were processed immunohistochemically for β3-tubulin, NF-200, and SMI312 collectively, P0 and YFP. High-power (63×) images were captured to encompass the spinal cord section at the lesion epicenter (week 12 uninjured control, $n = 4$; 1 wpi, $n = 5$; 3 wpi, $n = 6$; 12 wpi, $n = 7$), and P0+/YFP+/^{NEG} myelin sheaths were counted. In addition, recombination efficiency was assessed by counting the number of P0+ tubes that were colabeled with YFP in three consecutive T9/T10 dorsal and ventral root sections in uninjured control *P0-CreER^{T2}:Rosa26-eYFP* mice ($n = 4$). An average of 600 cells was counted per uninjured mouse.

Experimental design and statistical analysis

Generally, male or female mice were given tamoxifen at 8–10 weeks of age and then sustained a SCI, dorsal root, or sciatic nerve injury at 10–12 weeks of age and tissue was harvested at different points post-injury (see Surgical procedures for specific details). Mouse lines are defined in Table 1, overall animal numbers are outlined in Table 2, and specific animal numbers for each quantification are outlined in the Methods section. Imaging and cell counts were performed on a Zeiss AxioObserver.Z1 inverted confocal microscope equipped with a Yokogawa spinning disk and Zen 2012 software (RRID: SCR_013672). Investigators were blinded to the animal identity (i.e., uninjured control or post-injury time point). All data are reported as means ± SEM using GraphPad Prism 5 (RRID: SCR_002798). For all analyses, quantifications were completed on cross-sectional tissue and the significance was tested using SPSS software (IBM; RRID: SCR_002865) and measured using the Kruskal–Wallis test with a follow up Mann–Whitney *U* test (reported in figure legends) and considered significant if $p < 0.05$.

Results

Genetic fate mapping identifies PDGFRα progeny in the adult spinal cord

We systematically assessed the ability of different cell types to form myelinating cells in response to SCI using seven transgenic mouse lines. Due to the inducible nature of Cre recombinase by tamoxifen in the main six mouse lines used for *in vivo* fate mapping experiments, cells were labeled before injury with no additional recombination taking place after SCI. Animals were

Table 3. Primary antibody table

Primary antibody	Used as a marker for	Host	Source, Catalog#, RRID	Ratio; IHC/ICC
APC (CC1 Clone)	Oligodendrocytes	Mouse, IgG2bκ	Calbiochem, OP80 RRID: AB_2057371	1:300; IHC
αSMA clone EPR5368	Fibroblast-like phenotype	Rabbit	Millipore, MABT381 RRID: AB_11203118	1:500; ICC
αSMA	Vascular-associated cells (type B pericytes as defined by Göritz et al., 2011)	Rabbit	Abcam, ab5694 RRID: AB_2223021	1:500; IHC
β3-tubulin (Tuj1)	Neural-specific tubulin	Mouse, IgG2bk	Sigma-Aldrich, T8660 RRID: AB_477590	1:1000; IHC
Contactin-associated protein (Caspr)	Paranodes	Rabbit	Abcam, ab34151 RRID: AB_869934	1:500; IHC
Fibronectin	Fibroblasts and extracellular matrix	Mouse	Sigma-Aldrich, F7387 RRID: AB_476988	1:400; IHC
GFAP	Reactive astrocytes	Rabbit	DAKO, Z0334 RRID: AB_10013382	1:1000; IHC
GFP	Reporter + cells (YFP + or GFP+)	Chicken	Abcam, ab13970 RRID: AB_300798	1:1000; IHC
GFP	Reporter + cells (YFP + or GFP+)	Goat	Rockland, 600-101-215 RRID: AB_218182	1:500; IHC
GFP	Reporter + cells (YFP + or GFP+)	Rabbit	Abcam, ab290 RRID: AB_303395	1:6000; IHC
GFP	Reporter + cells (YFP + or GFP+)	Rat	Nacalai tesque, 04404-84 RRID: AB_10013361	1:1000; IHC
GFP	Reporter + cells (YFP + or GFP+)	Mouse, IgG1	Millipore, mab3580 RRID: AB_94936	1:500; IHC
Glut1	Endothelial cells	Goat	Santa Cruz, sc-1605 RRID: AB_2239463	1:200; IHC
Krox 20 (Egr2)	Myelinating Schwann cells	Rabbit	Covance PRB-236P RRID: AB_291594	1:500; IHC
Laminin	Basal lamina, extracellular matrix	Rabbit	Sigma-Aldrich, L9393 RRID: AB_477163	1:200; IHC
MBP	Myelin	Chicken	Aves, MBP RRID: AB_2313550	1:200; IHC
MBP	Myelin	Goat	Santa Cruz Biotechnology, sc-13914 RRID: AB_648798	1:500; IHC
MYRF, GM98 (N-terminus)	Differentiated oligodendrocytes	Rabbit	Gift from Dr. Wegner	1:500; IHC
Nestin, clone 2Q178	consistent with an immature/ proliferative Schwann cell phenotype	Mouse	Santa Cruz Biotechnology, sc-58813 RRID: AB_784786	1:500; ICC
Neurofilament 200	Heavy chain neurofilaments	Mouse, IgG1	Sigma-Aldrich, N0142 RRID: AB_477257	1:1000; IHC
NG2	Oligodendrocyte precursors	Rabbit	Millipore, AB5320 RRID: AB_11213678	1:200; IHC
Olig2	Oligodendrocyte precursors and oligodendrocytes	Rabbit	Millipore, AB9610 RRID: AB_10141047	1:300; IHC
P0	Myelinating Schwann cells, peripheral myelin	Chicken	Aves, PZ0 RRID: AB_2313561	1:100; IHC
P75NTR	Consistent with an immature/ proliferative Schwann cell phenotype	Rabbit	Millipore, AB1554 RRID: AB_11211656	1:200; ICC
P75NTR	Non-myelinating Schwann cells	Rabbit	Sigma-Aldrich, N3908 RRID: AB_260763	1:100; IHC
PDGFRα	Oligodendrocyte precursors, type A pericytes (as defined by Göritz et al., 2011)	Goat	R&D Sytems, af1062 RRID: AB_2236897	1:100; IHC
PDGFRβ	Type A pericytes (as defined by Göritz et al., 2011)	Rabbit	Abcam, ab32570 RRID: AB_777165	1:100; IHC
Reca 1, clone HIS52	Endothelial cells	Mouse, IgG1	Serotec, MCA970R RRID: AB_323297	1:500; IHC
SMI312	Pan neurofilaments	Mouse	Covance, SMI-312R-100 RRID: AB_509993	1:1000; IHC
Sox2	Consistent with an immature/ proliferative Schwann cell phenotype	Rabbit	Stemgent, 09-0024 RRID: AB_2195775	1:200; ICC

allowed to survive for 3 or 12 weeks after SCI. The first goal of our study was to obtain an estimate of the amount of new myelin formation following SCI and determine its cellular origin. As it is widely accepted that oligodendrocytes are produced via the differentiation of OPCs, we performed OPC fate mapping with two independent mouse lines driving the expression of a tamoxifen-inducible Cre recombinase under the PDGFRα promoter: *PDGFRα-CreER* mice [Kang et al., 2010; denoted throughout as *PDGFRα-CreER(I)*] and *PDGFRα-CreER*^{T2} mice (Rivers et al., 2008; denoted throughout as *PDGFRα-CreER(II)*].

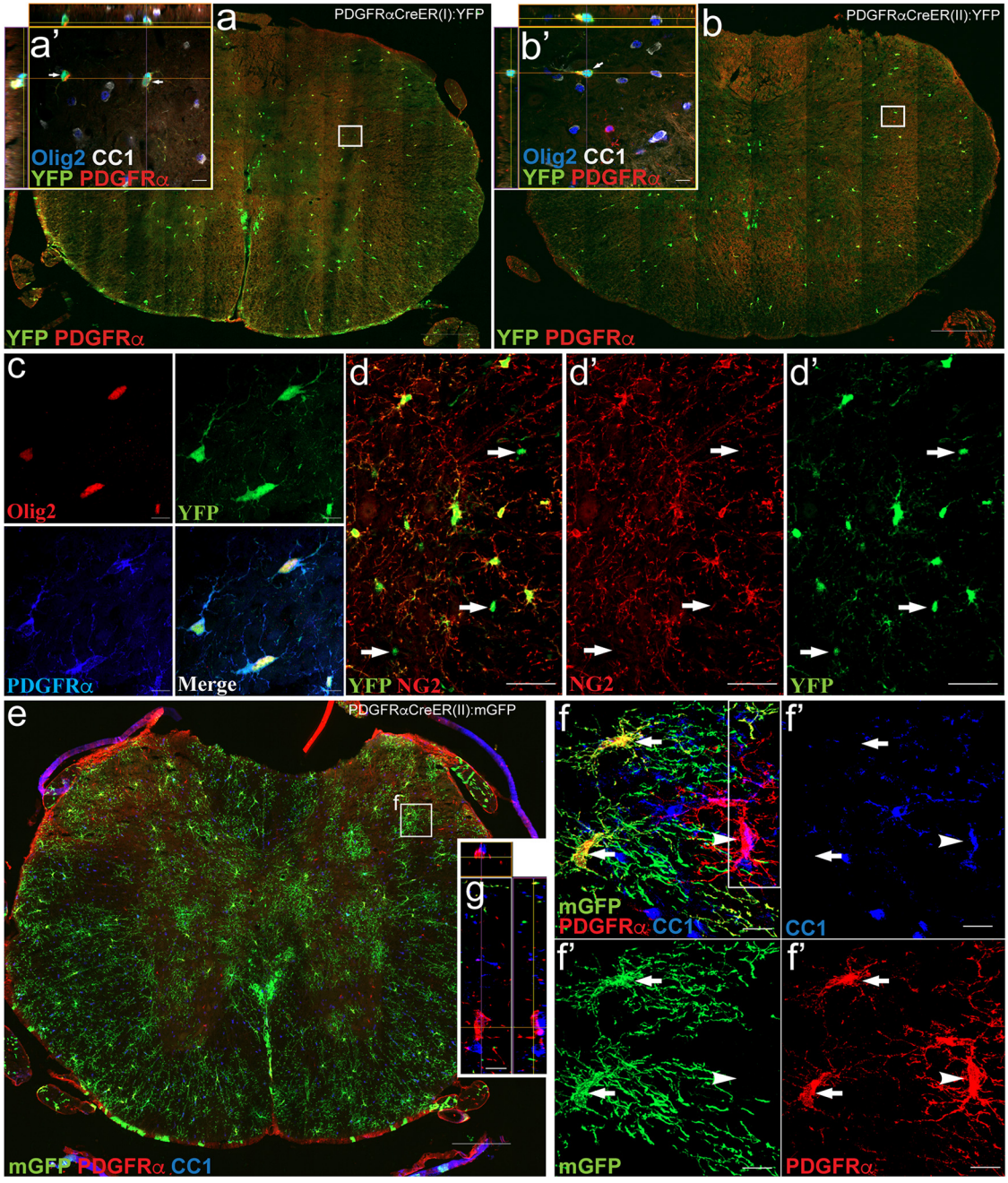

Figure 1. Genetic labeling of NG2 glia in tamoxifen-inducible *PDGFRαCreER* uninjured control mice. ***a***, ***b***, After the 2 week tamoxifen washout period, Tamoxifen-induced YFP expression in the cytoplasm was observed in two independent P*DGFRαCreER* mouse lines (I and II) crossed to the YFP reporter line. The majority of PDGFRα+ (red)/Olig2+ (blue) cells exhibited recombination (green) in *PDGFRαCreER(I):YFP* mice (***a***, ***a′***); recombination was more modest in *PDGFRαCreER(II):YFP* mice (***b***, ***b′***) when observed in uninjured control mice at 14 d post-tamoxifen treatment. ***c***, ***d***, In both lines, YFP (green), Olig2 (red), and PDGFRα (blue) were coexpressed (***c***), and the recombined population of cells was also coexpressed with the NG2+ (red) population. Arrows point to rare examples of GFP+ cells not overlapping with NG2+ cell (***d***). ***e***, *PDGFRαCreER* mice were crossed with membrane-tethered (mGFP; green). ***f***, 3D rendering at 14 d after tamoxifen treatment, the majority of PDGFRα+ cells are recombined (mGFP+; green, arrows) with a small subset of PDGFRα+ cells not recombined (arrowhead). It was rare to find recombined cells that had matured into an oligodendrocyte (CC1+; blue) at time of injury. ***g***, Confocal image including Z-plane from outlined box in ***f*** demonstrating that PDGFRα does not overlap with CC1 (blue) cells but it is two independent cells on top of one another. All images were taken in spinal cord cross sections. Scale bars: ***a***, ***b***, ***e***, 200 μm; ***d***, 50 μm; ***a′***, ***b′***, ***c***, ***f***, 10 μm .

We examined the extent and identity of recombined cells (defined as cells that were PDGFRα promoter active cells at the time of tamoxifen dosing and hence positive for YFP or mGFP) in the adult uninjured control *PDGFRα-Cre:-YFP* or *-mGFP* mice. Tamoxifen was administered at 8–10 weeks of age, and recombination in the spinal cord with the attached dorsal roots was examined 14 d later (Figs. 1, 2). In all four mouse lines, tamoxifen-induced Cre activation induced abundant and robust expression of YFP or mGFP. The *PDGFRα-CreER(I):Rosa26-mGFP(mT/mG)* and *PDGFRα CreER(II):Rosa26-eYFP* mouse lines were investigated to confirm observations made in separate mouse lines but no quantification was performed in these mice. Oligodendrocyte lineage cells are identifiable by characteristic protein expression: Olig2 is expressed in both OPCs and mature oligodendrocytes, whereas PDGFRα and NG2 are expressed in OPCs, and CC1 and myelin regulatory factor (MYRF)

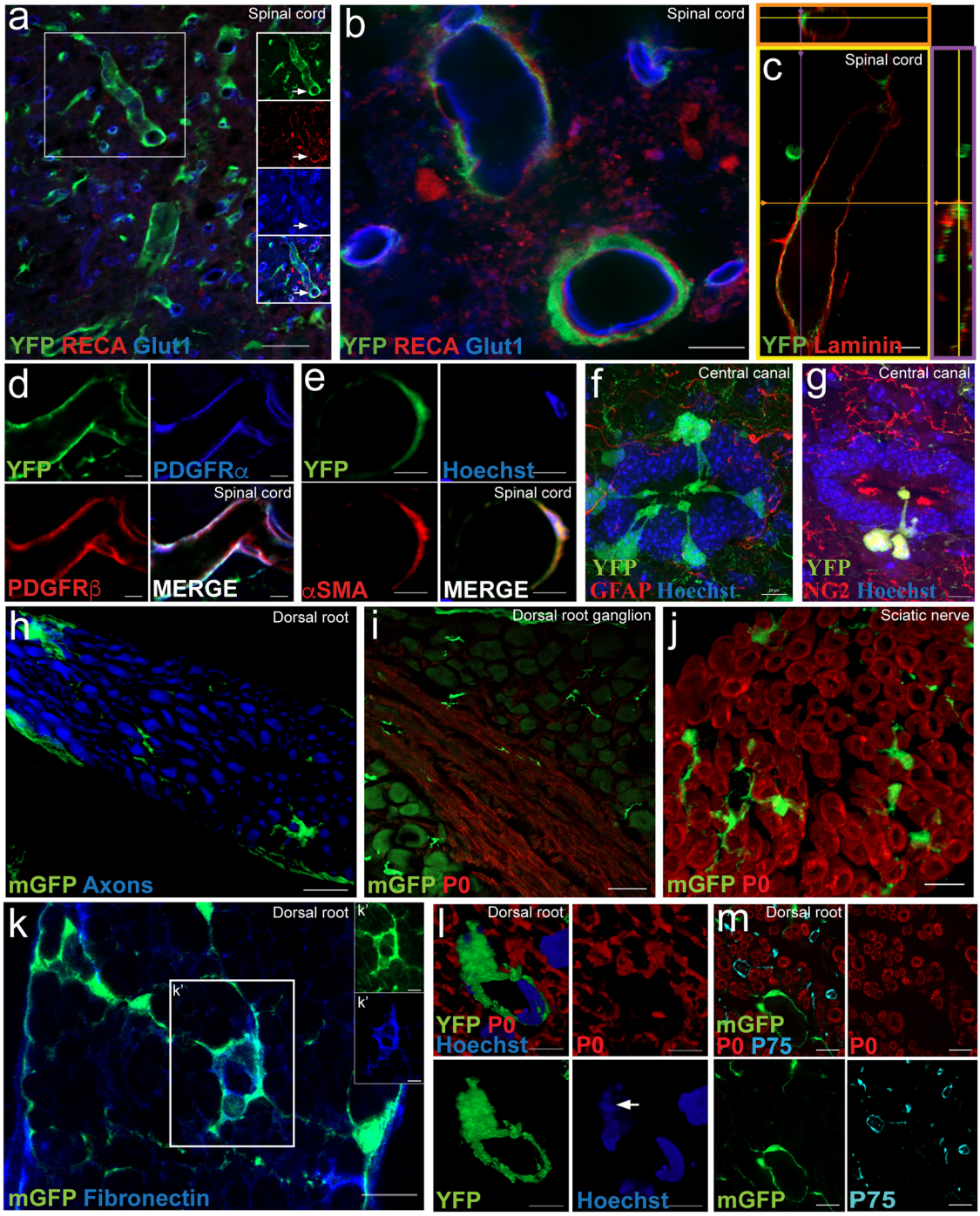

Figure 2. Recombination in central canal-associated cells, vascular associated cells and a subset of PNS endoneurial cells in *PDGFRαCreER* uninjured control mice. ***a***, ***b***, In the uninjured spinal cord of *PDGFRαCreER:YFP* or *mGFP* mice, recombination (green) was observed in a subset of blood vessel-associated cells (arrow) located on the outside of the endothelial layer (RECA, red; Glut1, blue) but inside the outer basal lamina, (red; ***c***) consistent with the location of pericytes. The majority of the YFP-expressing vascular-associated cells expressed PDGFRα (blue; ***d***) and PDGFRβ (red; ***d***), referred to previously as type A pericytes. A small subset of the YFP+ vascular associated cells appeared to coexpress of YFP (green) and αSMA (red; ***e***; referred to previously as a type B pericytes marker). ***f***, ***g***, Recombination can also be seen in a small number of cells located peripherally in the wall of the central canal, each with a process extending into the lumen of the canal (***f***); these cells were also NG2+ (red; g). ***h–l***, A subset of endoneurial cells and pericytes (green) that exhibited recombination (i.e., YFP+ or mGFP+) were found in the dorsal root (***h***), DRG (***i***), and sciatic nerve (***j***) in the uninjured PNS in both lines of *PDGFRαCreER*. Many recombined cells in the dorsal root coexpressed fibronectin (blue; ***k***). Rarely were YFP+ pericyte cell bodies encountered (e.g., arrow, nucleus, 3D rendering; ***l***) with associated processes encircling blood vessels in the dorsal root. ***m***, Importantly, recombined cells in the dorsal root did not coexpress the non-myelinating Schwann cell marker p75 (cyan; ***m***), or the myelinating Schwann cell marker P0 (red; ***i***, ***j***, ***l***, ***m***). All images were taken in spinal cord cross section. Scale bars: ***a***, 100 μm; ***i***, 50 μm; ***b***, ***c***, ***f***, ***g***, ***h***, ***j***, ***k***, ***m***, 10 μm; ***d***, ***e***, ***l***, 5 μm.

are specific to oligodendrocytes (Kitada and Rowitch, 2006; Emery et al., 2009; Bujalka et al., 2013). Example images taken 2 weeks after tamoxifen induction, at the time when the injury would have been inflicted, demonstrate YFP colabeling with OPC markers PDGFRα/Olig2 (Fig. 1*a–c*) and NG2 (Fig. 1*d*), in cells that have a typical OPC morphology visualized with the membrane-tethered reporter (Fig. 1*e*,*f*). The recombination efficiency at the time of injury (number of nonvascular GFP+

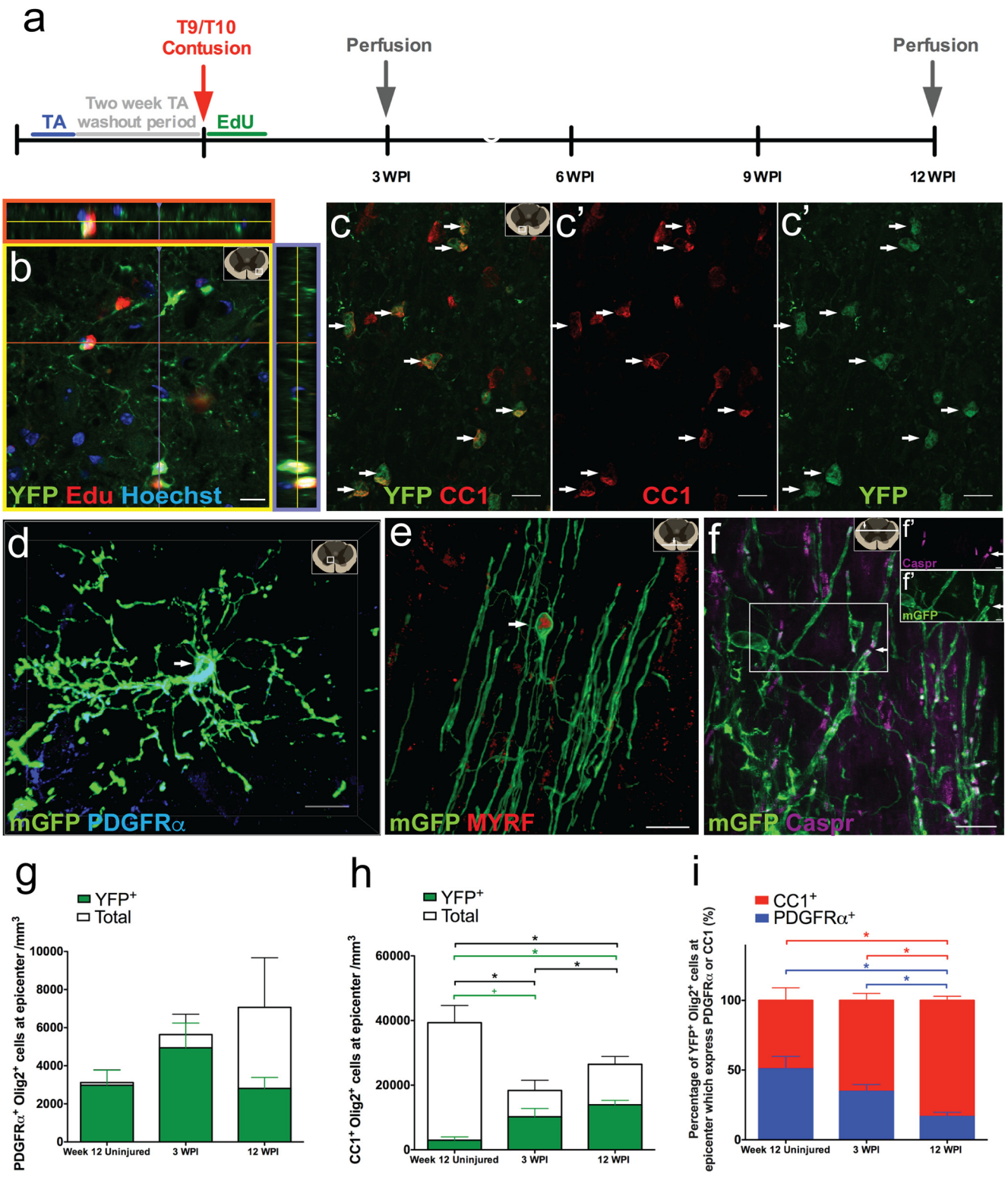

Figure 3. PDGFRα+ progenitors proliferate and contribute to oligodendrocyte lineage cells in response to SCI. ***a***, Timeline for SCI experiment. Tamoxifen was administered to 8- to 10-week-old mice; mice were given a 2 week tamoxifen washout period before a T9/T10 contusion SCI. Twelve weeks after SCI, recombined YFP+ cells incorporated EdU (red; ***b***) and many recombined cells (green) differentiated into CC1-expressing (red) oligodendrocytes (***c***, arrow). Note the schematic in top right corner of images indicates approximate location where image was taken based on spinal cord cross section. Using the mGFP reporter mice, a small subset of recombined cells continue to express PDGFRα (blue; ***d***, arrow), whereas the majority of recombined cells are now oligodendrocytes with extended processes ensheathing/myelinating axons and expressing MYRF (red; ***e***, arrow). ***f***, mGFP+ oligodendrocytes expressed the paranodal marker Caspr (arrows) with split channels (***f′***). There were no differences observed in the overall number of OPCs (PDGFRa+Olig2+) or recombined OPCs (YFP+PDGFRa+Olig2+) across the groups (***g***). ***h***, The amount of total oligodendrocytes and new YFP+ oligodendrocytes differed significantly among the groups ($\chi^2_{(2)} = 8.57, p = 0.014$ and $\chi^2_{(2)} = 6.18, p = 0.045$, respectively). There was a decrease in the overall oligodendrocytes (CC1+Olig2+) at 3 and 12 wpi compared with the week 12 uninjured group ($U_{(5)} = 0.00, p = 0.034$ and $U_{(7)} = 1.00, p = 0.039$, respectively; ***h***). There were more overall oligodendrocytes at 12 wpi compared with 3 wpi ($U_{(8)} = 2.00, p = 0.033$; ***h***). There were more new oligodendrocytes (YFP+CC1+Olig2+) at 12 wpi compared with the week 12 uninjured group ($U_{(7)} = 0.00, p = 0.020$; ***h***) but the difference observed between the week 12 uninjured group and 3 wpi did not reach significance ($U_{(5)} = 1.00, p = 0.07$; ***h***). ***I***, Among the total (*Figure legend continues.*)

PDGFRα+ cells divided by the total number of nonvascular PDGFRα+ cells) in the spinal cord of *PDGFRα-CreER(I):YFP* and *PDGFRα-CreER(II):mGFP* mice was 85 ± 2% and 69 ± 1%, respectively.

In addition to cells in the oligodendrocyte lineage, tamoxifen-induced recombination was also observed to a lesser extent in other PDGFRα-expressing cells in both *PDGFRα-CreER:YFP* or *mGFP* mice lines. Within the CNS, we encountered recombination in vascular-associated cells (Fig. 2*a–e*). Blood vessel-associated cells expressing YFP were located on the outside of the endothelial layer (delineated by RECA and Glut1; Fig. 2*a*,*b*) and on the inside of the outer basal lamina (Fig. 2*c*), consistent with the location of pericytes. The majority of YFP+ cells in this region expressed PDGFRα and PDGFRβ (Fig. 2*d*) which classifies them as type A pericytes (Göritz et al., 2011). A second small subset of YFP+ vascular-associated cells appeared to also express the vascular-associated cell marker αSMA (Fig. 2*e*; defined as type B pericytes by Göritz et al., 2011). We occasionally observed recombination in some central canal-associated cells, whose cell bodies were located immediately outside of the ependymal layer with a process extended toward the lumen of the canal (Fig. 2*f*,*g*).

In the PNS, recombined cells in *PDGFRα-CreER:-YFP* or *-mGFP* mice were found in the dorsal root (Fig. 2*h*), DRG (Fig. 2*i*), and sciatic nerve (Fig. 2*j*). These GFP+ cells in the PNS are endoneurial cells and expressed fibronectin (Fig. 2*k*). YFP+ vascular-associated cell bodies were also encountered in the PNS (Fig. 2*l*), with associated processes encircling blood vessels in the dorsal root. Importantly, recombined cells in the dorsal root did not coexpress the myelinating Schwann cell marker P0, or p75 which is typically expressed in non-myelinating Schwann cells (Fig. 2*i*,*j*,*l*,*m*).

PDGFRα+ cells, recombined before injury, contribute to new oligodendrocyte ensheathment/myelination after SCI

To estimate the amount of new ensheathment/myelin formed by endogenous oligodendrocytes after SCI, we performed lineage tracing of OPCs in *PDGFRα-CreER:-YFP* or *-mGFP* mice recombined before injury (Fig. 3*a*). Twelve weeks after SCI, YFP+ cells had retained EdU (Fig. 3*b*), indicating that they proliferated in response to the trauma. In contrast to the uninjured scenario (at time of injury), where the majority of recombined cells coexpressed PDGFRα and NG2 (indicating they are OPCs; Fig. 1), most of the recombined cells at 12 weeks after SCI coexpressed CC1 (identifying them as new oligodendrocytes; Fig. 3*c*). In mGFP mice (i.e., carrying the membrane-tethered reporter), recombined cells with the morphological features of both OPCs and oligodendrocytes were highly enriched around the injury site, and these cells were also encountered at great distances from the injury epicenter. These morphological cellular features of recombined cells correlated with immunohistochemical profiling: OPCs characterized by ramified processes and the expression of PDGFRα (Fig. 3*d*) and a larger percentage of mature oligodendrocytes with tube formation and rostro-caudally aligned processes also expressed the transcription factor MYRF which is essential for myelination (Fig. 3*e*; Emery et al., 2009; Koenning et al., 2012). Crucially, the expression of the contactin-associated protein (Caspr) in the axonal-glial contacts of the paranodes could be easily colabeled with mGFP+ tubes, indicative of the presence of Ranvier nodes and suggestive of oligodendrocyte ensheathment and ongoing myelination (Fig. 3*f*).

To quantify the extent of new oligodendrocytes formed after SCI, we performed analysis in *PDGFRα-CreER(I):YFP* mice and coimmunostained Olig2+ cells for either, PDGFRα (OPCs) or CC1 (oligodendrocytes), and counted their total number and their number also staining for YFP+ (recombined cells). Recombined YFP+ cells colabeling with Olig2 and PDGFRα represent OPCs and colabeling with Olig2 and CC1 is indicative of differentiation into oligodendrocytes. There was no difference observed following injury in the density of total OPCs (PDGFRα+ Olig2+cells) nor in the recombined subpopulation of OPCs (YFP+PDGFRα+Olig2+; Fig. 3*g*). In contrast, there were significantly more oligodendrocytes at 12 wpi compared with 3 wpi (Fig. 3*h*). Presumably this increase in new oligodendrocytes was due to OPC differentiation into new oligodendrocytes as there were more new oligodendrocytes (YFP+CC1+Olig2+) at 12 wpi compared with the 12 week uninjured control group (Fig. 3*h*). We found that oligodendrocytes continued to differentiate between 3 and 12 wpi as there was a higher percentage of recombined new oligodendrocytes (83%) compared with 3 wpi (65%) and the week 12 uninjured groups (49%) (Fig. 3*i*). Reciprocally, the 12 wpi group showed the lowest percentage of recombined OPCs (17%) compared with the 3 wpi (35%) and week 12 uninjured groups (51%; Fig. 3*i*) in the recombined oligodendrocyte lineage (YFP+Olig2+). Further, our data reveal that there is a fivefold increase in the amount of new oligodendrocytes at 12 wpi (13,929 ± 1356) compared the 12 week uninjured control group (2978 ± 1031) and that 53% of the epicenter oligodendrocytes at 12 wpi are from new YFP+ oligodendrocytes (Fig. 3*i*). Collectively, these data demonstrate that following SCI there is considerable oligodendrogenesis from PDGFRα+ OPCs recombined before injury, and this is a prolonged process after SCI.

To determine the extent of ensheathment/myelination by recombined PDGFRα+ cells, we performed quantitative analyses in *PDGFRα-CreER(II):mGFP* mice using cross-sections of the spinal cord from animals 3 or 12 wpi and uninjured age-matched controls (Fig. 4). At 3 and 12 wpi, mGFP+ cells could be visualized extending processes that surrounded nearby axons but only some of these mGFP+ tubes colabeled with MBP (Fig. 4*a*,*b*). Following a moderate-severe contusion SCI, there was a ~75% reduction in the number of MBP+ myelin sheaths remaining at 3 and 12 weeks after SCI compared with the uninjured age-matched spinal cord (Fig. 4*c*). By 3 weeks post-SCI there were newly generated oligodendrocyte-derived myelin sheaths (i.e., in mGFP+MBP+P0^{NEG} cells); the production of new oligodendrocyte-derived myelin sheaths continued as the percentage of these newly generated sheaths increased by 12 wpi (Fig. 4*d*). The percentage of new myelin produced by oligodendrocytes accounted for ~20% of the total myelinated axons at the epicenter (i.e., mGFP+) by 12 wpi. This percentage of newly myelinated axons represents an underestimate, because recombination efficiency in this mouse line was only 68% (calculated during initial mouse characterization). When we account for this recombination efficiency we estimate that *de novo* myelin generation at injury epicenter by 12

←

(*Figure legend continued.*) YFP+Olig2+ population, the percentages of oligodendrocytes (YFP+CC1+Olig2+) and the percentages of OPCs (YFP+PDGFRα+Olig2+) differed significantly among the groups ($\chi^2_{(2)} = 8.27$, $p = 0.016$; $\chi^2_{(2)} = 8.27$, $p = 0.016$, respectively). Among the total YFP+Olig2+ population, there was a higher percentage of oligodendrocytes (YFP+CC1+Olig2+) at 12 wpi compared with both 3 wpi ($U_{(8)} = 2.00$, $p = 0.033$) and the week 12 uninjured control group ($U_{(7)} = 0.00$, $p = 0.02$; ***i***). Reciprocally, there was a lower percentage of OPCs (YFP+PDGFRα+Olig2+) at 12 wpi compared with the 3 wpi ($U_{(8)} = 2.00$, $p = 0.033$) and the week 12 uninjured control group ($U_{(7)} = 0.00$, $p = 0.02$; ***i***). Images were taken in both epicenter spinal cord cross sections (***b–d***) and longitudinal sections (***e***) near epicenter. *$p < 0.05$; +$p < 0.1$. Scale bars: ***b***, ***c***, 20 μm; ***e***, 15 μm; ***d***, ***f***, 10 μm; ***f′***, 2 μm. Error bars represent the SEM.

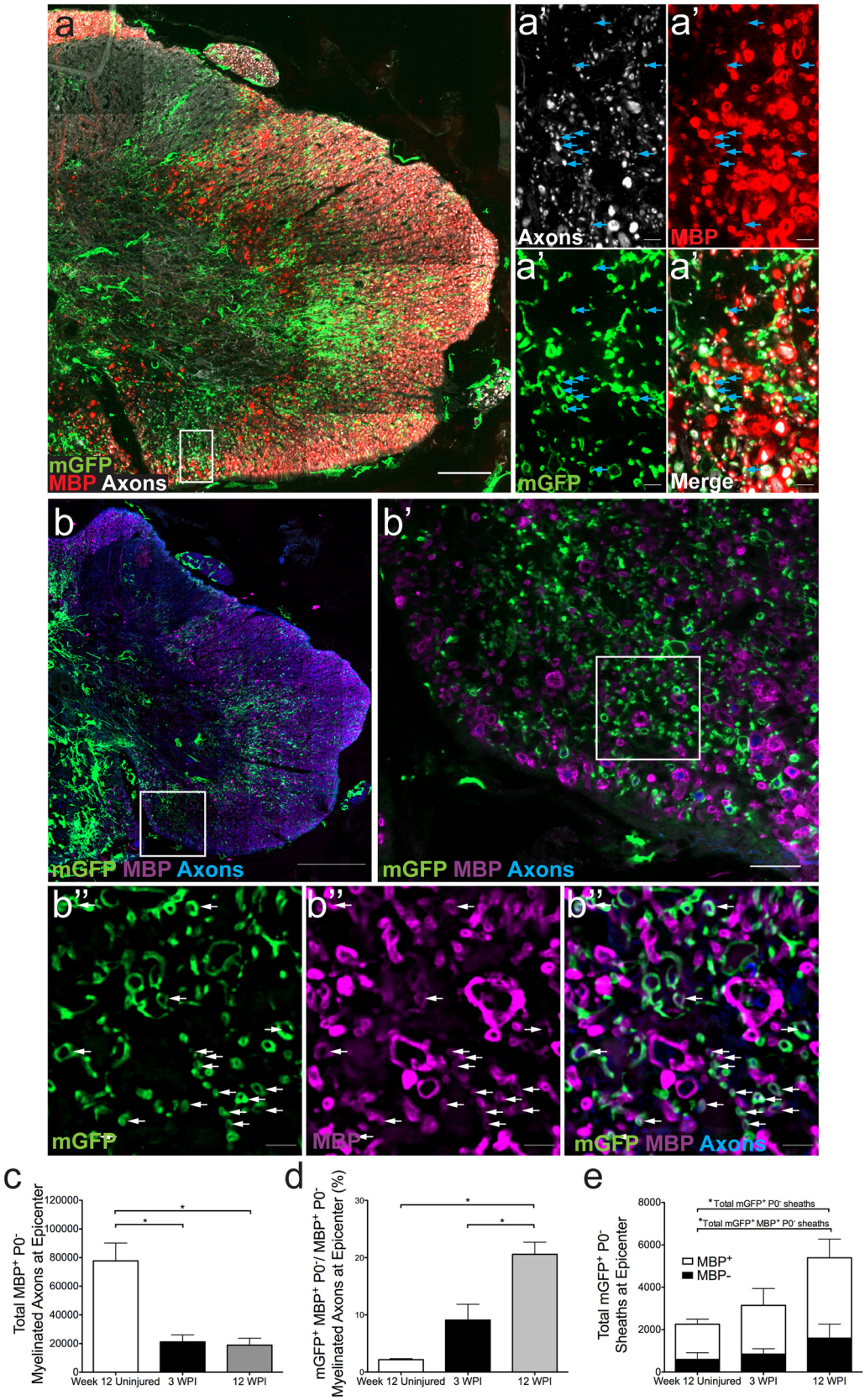

Figure 4. Extensive new ensheathment/myelination by oligodendrocytes derived from PDGFRα+ progenitors 12 weeks after SCI. Twelve weeks after contusion injury, large numbers of membrane-bound mGFP+ tubes (green) were observed in *PDGFRαCreER (II):mGFP* mice indicating new ensheathment/myelination (***a***, ***b***). Slides were stained with antibodies for axons (***a***, white; ***b***, blue), MBP (***a***, red; ***b***, purple), mGFP (green), and P0 (data not shown). Note that some images are displayed as flattened images (combining large numbers of *z*-stacks into one image; ***a***, ***b***, ***b′***), whereas others are a single *z*-stack image (a confocal optical section; ***a′***, ***b″***). A proportion of sheaths coexpressed MBP [***a′***, ***b″***; single optical plane at higher-magnification; arrows denote clear mGFP+ (green) and MBP+ (red or purple) tubes]. ***c–e***, Quantification of axons myelinated by oligodendrocytes after SCI (i.e., MBP+, P0^{NEG} processes) at the (*Figure legend continues.*)

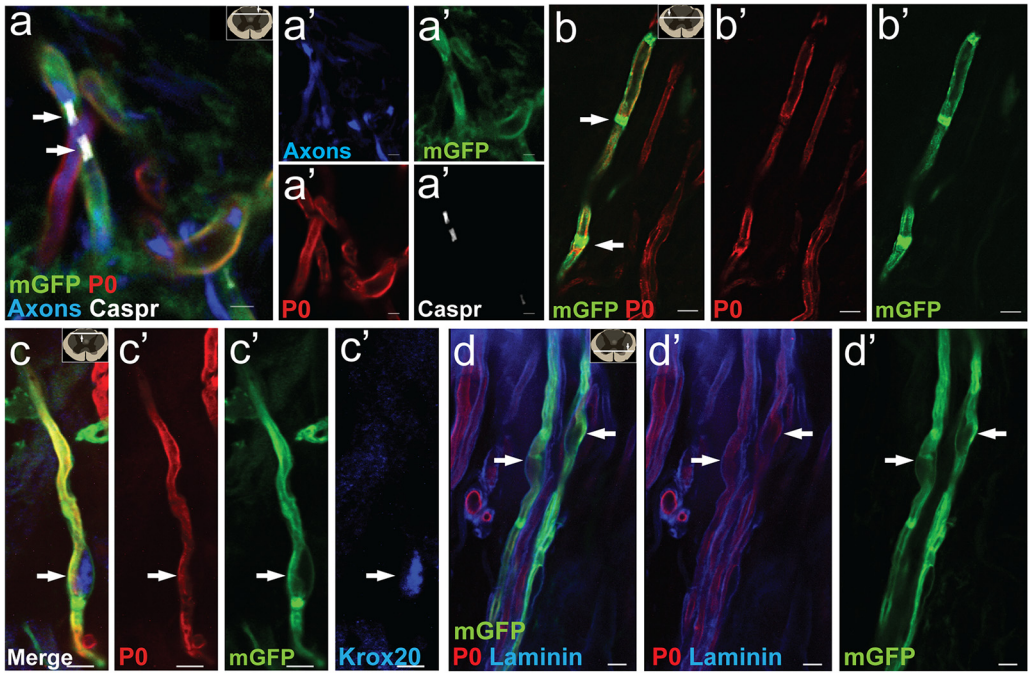

Figure 5. PDGFRα+ progenitor-derived Schwann cells express typical hallmarks of Schwann cell myelination in *PDGFRαCreER:mGFP* mice. ***a***, ***b***, Arrows point to paranodal marker Caspr (white; ***a***) and to Schmidt-Lanterman incisures (area where myelin is less compact allowing an accumulation of GFP antibody and a decrease in P0; ***b***, arrows); both indicative of mature nodes of Ranvier and myelination. ***c***, ***d***, 12 weeks after injury, recombined myelinating Schwann cells expressed the transcription factor Krox20 (***c***, arrow) and were surrounded by a basal lamina (***d***, arrows point to cell body), both hallmarks of myelinating Schwann cells. All images taken in spinal cord longitudinal sections near epicenter. Scale bars: ***b***–***d***, 5 μm; ***a***, 3 μm.

weeks after SCI approaches 30%. To our surprise, even at 12 wpi approximately one-third of these mGFP+ rings surrounding axons did not reveal detectable MBP expression, suggesting that mGFP+ tubes label either OPC processes engaging with axons or early oligodendrocyte ensheathment (MBP^{NEG}; Fig. 4*e*). *De novo* myelin production in the uninjured age-matched spinal cord was much slower and 2.16% of the MBP+P0^{NEG} myelin sheaths were mGFP+, i.e., newly generated over a comparable period of 12 weeks (Fig. 4*d*). Together, these data demonstrate that there is a 6- to 10-fold increase in *de novo* myelination at the lesion epicenter in the 3 months following SCI compared with uninjured age-matched controls.

The majority of myelinating Schwann cells in the injured spinal cord are derived from PDGFRα+ cells

Schwann cell myelination is prominent following contusive SCI, and PDGFRα+ cells have been show to produce myelinating Schwann cells following chemical demyelination (Zawadzka et al., 2010). To determine whether PDGFRα+ cells are also responsible for Schwann cell myelination, we examined the expression of myelinating Schwann cell markers in recombined cells of *PDGFRα-CreER:-YFP* or *-mGFP* mice. In *PDGFRα-CreER:mGFP* mice the membrane-tethered reporter allowed us to readily visualize coexpression of mGFP and P0 in myelin tubes after SCI, suggesting that PDGFRα+ cells gave rise to myelinating Schwann cells after contusion SCI (Fig. 5*a*–*d*, arrows). Twelve weeks after SCI, PDGFRα+ progenitor-derived Schwann cell tubes exhibited many characteristics of mature Schwann cell myelin including the expression of Caspr in the axonal-glial contacts of the paranodes (Fig. 5*a*) as well as the formation of Schmidt-Lanterman incisures (Fig. 5*b*). Although this was not quantified, example images revealed that recombined myelinating Schwann cells expressed the transcription factor Krox20 (Fig. 5*c*) and were surrounded by a basal lamina staining for laminin (Fig. 5*d*), both hallmarks of myelinating Schwann cells. Importantly, P0+, PDGFRα-derived myelin was abundant in both independent *PDGFRα-CreER* mouse lines (i.e., lines I and II) after SCI and PDGFRα-fate mapping did not label Schwann cells in the peripheral nerve (Fig. 2*h*–*m*).

We next examined the distribution and contribution of OPC-derived myelinating Schwann cell profiles in the *PDGFRα-CreER:-YFP* or *-mGFP* mice to the myelination of axons at the SCI epicenter (Fig. 6*a*–*d*,*f*). We observed that the P0+ Schwann cell myelin was most concentrated in the dorsal regions of the cord near the injury epicenter. Due to the nature of the dorsal contusion injury, the cytoarchitecture of the spinal cord was most disrupted within the lesion core and in the dorsal column regions, indicated by sparse glial fibrillary acidic protien (GFAP) staining (Fig. 6*a*′). Twelve weeks after SCI, these dorsal areas of substantial astrocyte loss were populated by YFP+ myelin sheaths that also expressed the Schwann cell-specific myelin

←

(*Figure legend continued.*) lesion epicenter demonstrated group differences ($\chi^2_{(2)} = 6.37$, $p = 0.041$; ***c***) with significantly less myelinated axons at 3 and 12 wpi compared with uninjured age-matched controls ($U_{(5)} = 0.00$, $p = 0.034$ and $U_{(6)} = 0.00$, $p = 0.025$, respectively; ***c***). The percentage of newly myelinated axons (surrounded by both mGFP+ and MBP+ tubes) to total myelinated axons (surrounded by just MBP+ tube) differed by group ($\chi^2_{(2)} = 8.48$, $p = 0.014$) and were significantly higher at 12 wpi compared with 3 wpi and uninjured age-matched controls ($U_{(7)} = 0.00$, $p = 0.014$ and $U_{(6)} = 0.00$, $p = 0.025$; ***d***). Quantification of MBP expression in mGFP+ sheaths indicative of new myelin (open portion of bar) and of MBP^{NEG} mGFP+ sheaths indicative of either OPC process wrapping or merely ensheathing oligodendrocytes (***e***, closed portion of bar). Quantification of total mGFP+P0^{NEG} sheaths (combined open and closed portion of bar) differed between groups ($\chi^2_{(2)} = 6.37$, $p = 0.041$) with significantly more overall mGFP+P0^{NEG} sheaths at 12 wpi compared with uninjured age-matched controls ($U_{(6)} = 0.00$, $p = 0.025$; ***e***). Quantification of MBP expression in mGFP+ sheaths indicative of new myelin (open portion of bar) differed between groups ($\chi^2_{(2)} = 6.37$, $p = 0.041$) with significantly more mGFP+MBP+P0^{NEG} tubes at 12 wpi compared with uninjured age-matched controls ($U_{(6)} = 0.00$, $p = 0.025$; ***e***). All images were taken in epicenter spinal cord cross sections. *$p < 0.05$. Scale bars: ***b***, 200 μm; ***a***, 100 μm; ***b′***, 20 μm; ***a′***, ***b″***, 5 μm. Error bars represent the SEM.

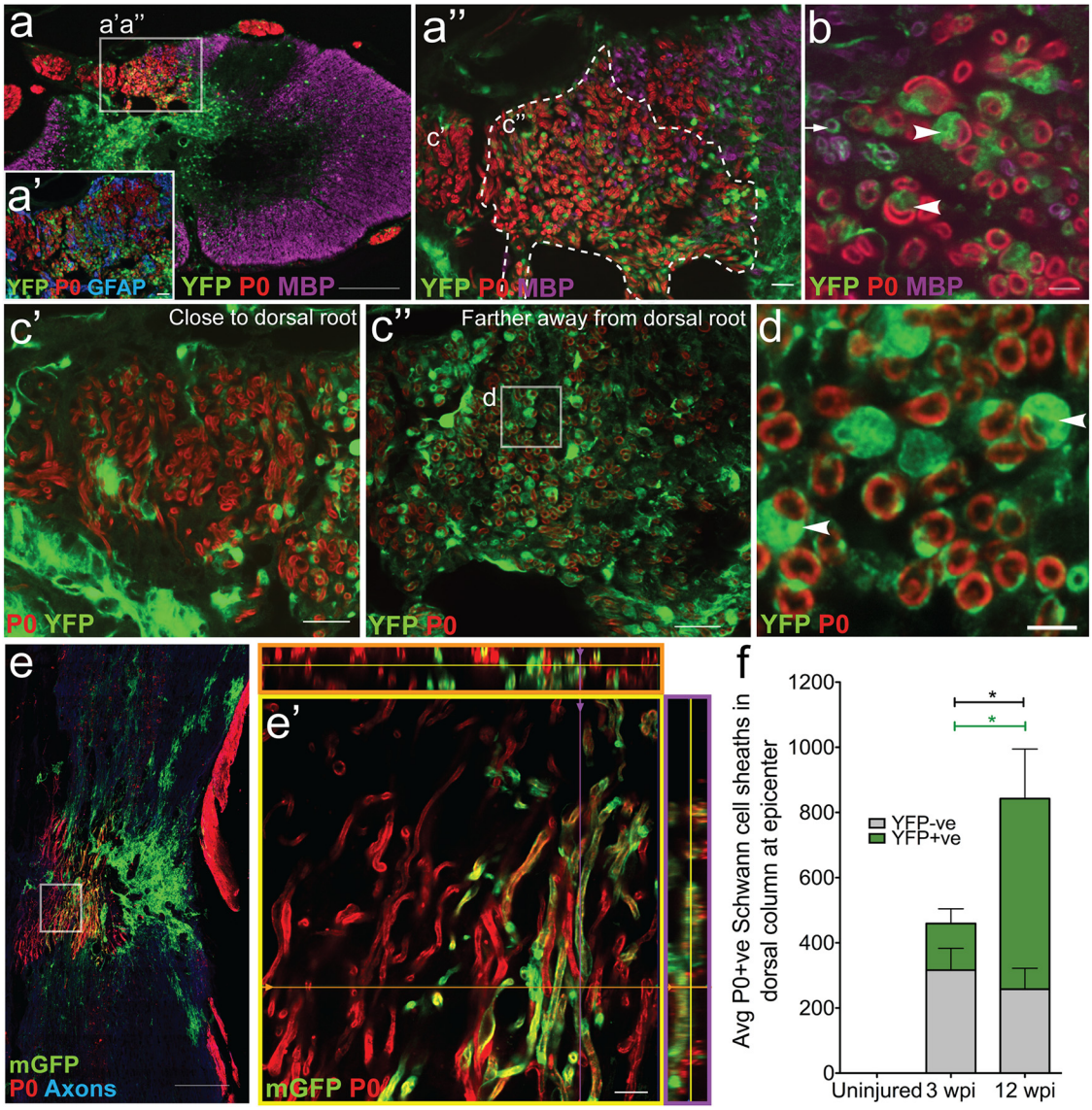

Figure 6. The majority of myelinating Schwann cells in the injured spinal cord are derived from PDGFRα+ progenitors. ***a***, Twelve weeks after spinal cord contusion in *PDGFRαCreER:YFP or mGFP* mice, P0+ (red) Schwann cell myelin was abundant within the dorsal columns in areas of substantial astrocyte loss. There were two distinct populations (***a''***) of P0+ myelin sheaths, a YFP^{NEG} population (***c'***) and a YFP+ population (***b***, ***c''***); most YFP^{NEG} P0+ myelin sheaths were found closer to the dorsal root entry zone, whereas the YFP+ P0+ sheaths were found mainly medially in the dorsal column (***c''***). ***b***, Arrowheads point to YFP+/P0+ myelin sheaths with the cell bodies of a Schwann cells in the image plane. The arrow denotes an oligodendrocyte ensheathed YFP+ nerve fiber. The arrowheads denote fibers with a clear one-to-one sheath-to-cell ratio typical for Schwann cells (***d***, arrowheads). ***e***, Schwann cell myelination was also apparent using the membrane-tethered reporter mGFP and horizontal sections through the lesion site (***e***, ***e'***; dorsal to the left). ***f***, The number of YFP+ myelinating Schwann cell profiles (green portion of bar) increased between 3 and 12 weeks after SCI ($U_{(12)} = 0.00$, $p = 0.001$). There were significantly more overall myelinating Schwann cell profiles (gray + green portion of bar) at 12 wpi compared with 3 wpi ($U_{(12)} = 8.00$, $p = 0.035$) and the majority of P0+ tubes were also YFP+. Images were taken in both epicenter spinal cord cross sections (***a–d***) and longitudinal sections near epicenter (***e***). *$p < 0.05$. Scale bars: ***a***, ***e***, 200 μm; ***c'***, ***c''***, ***a'***, ***a''***, 20 μm; ***e'***, 10 μm; ***b***, ***d***, 5 μm. Error bars represent the SEM.

marker P0 (Fig. 6*a*,*a'*,*a''*). Because Schwann cell myelin is surrounded by a thicker cytoplasmic outer wrapping compared with oligodendrocyte myelin, we were able to observe distinct recombined rings around Schwann cell-myelinated axons in both the YFP (Fig. 6*a–d*) and mGFP (Fig. 6*e*) reporter lines. Schwann cell myelin sheaths in the vicinity of the dorsal root entry zone were typically not derived from PDGFRα+ cells (i.e., were YFP^{NEG}; Fig. 6*c'*); in contrast, the medial dorsal columns contained many P0+ and YFP+ myelin sheaths (Fig. 6*c''*). Recombined P0+ myelin sheaths possessed morphological characteristics indicative of myelinating Schwann cells. For example, they myelinate axons with a one-to-one sheath-to-cell ratio (Fig. 6*d*, arrowheads) and expressed a basal lamina (Fig. 5*d*). Recombined myelinating Schwann cells were also observed in mGFP reporter mice (Fig. 6*e*,*e'*). The number of myelinating Schwann cell profiles derived from recombined PDGFRα progenitors (YFP+) in the injured spinal cord increased over time; by 12 weeks post-SCI, 67 ± 7.4% of the P0+ myelin coexpressed YFP suggesting an ongoing production of Schwann cells by PDGFRα progenitors after injury (Fig. 6*f*). In contrast, there was no change in the extent of ensheathment/myelination by peripherally derived (YFP^{NEG}) Schwann cells between 3 and 12 weeks post-SCI. The percentage of recombined myelinating Schwann cell profiles represents a slight underestimate considering that the recombination efficiency in this mouse line was 84%. After accounting for this recombination efficiency, we estimate that ~70–80% of the myelinating Schwann cell profiles at injury epicenter 12

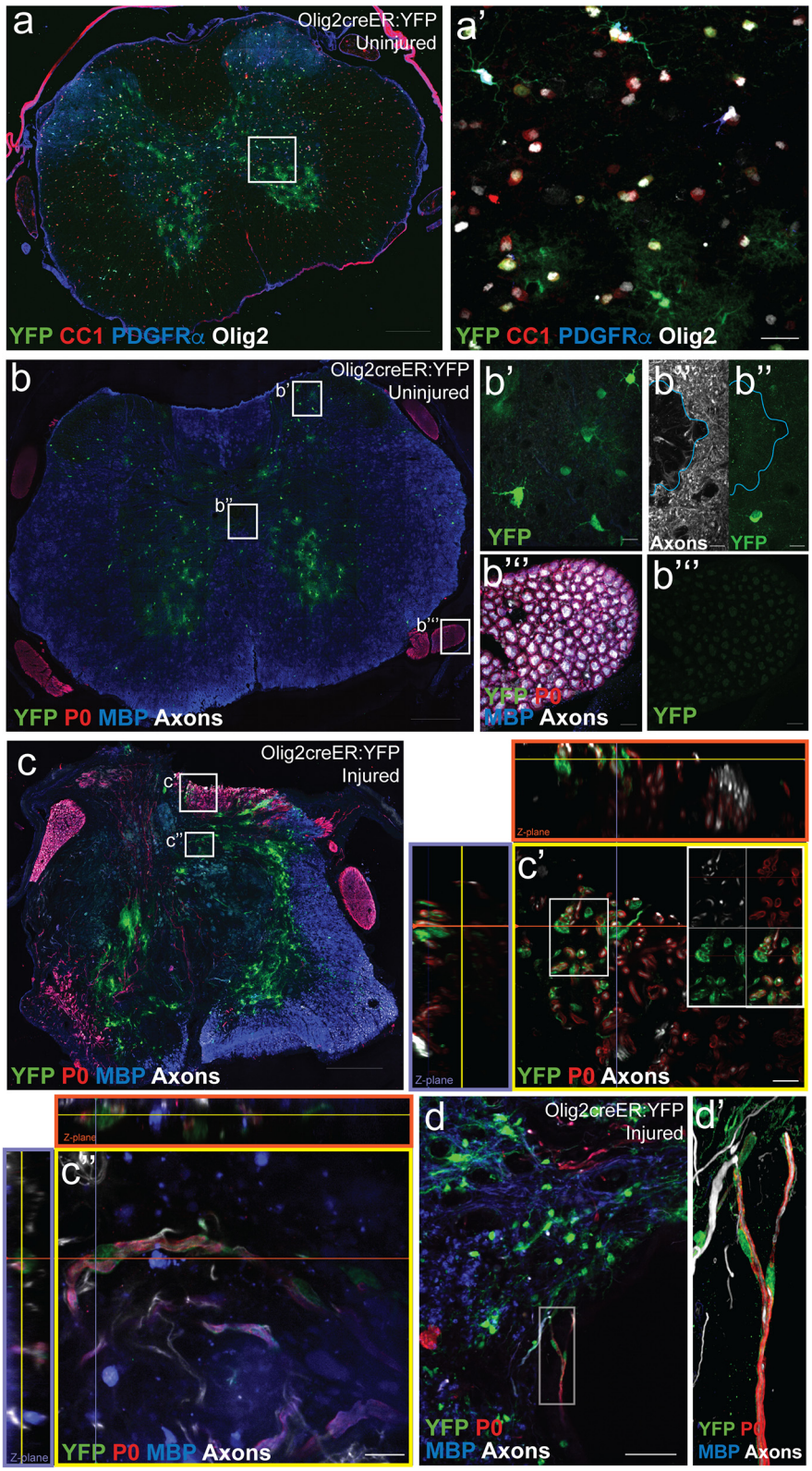

Figure 7. Olig2+ cells give rise to myelinating Schwann cells after SCI. *Olig2creER:YFP* mice were used to fate-map oligodendroglial lineage cells. ***a***, In the uninjured thoracic spinal cord, recombination (YFP; green) occurred in Olig2+ cells (white) across the oligodendrocyte lineage [preferentially observed in CC1+ oligodendrocytes (red) and to a lesser extent PDGFRα+ OPCs (blue)] and a subset of gray matter GFAP+ astrocytes. ***b***, There was no recombination observed in cells associated with the central canal [blue outline surrounds central canal; split channels with axons (white) and YFP (green); ***b''***] or the PNS (dorsal root; ***b'''***). ***c***, 12 weeks after SCI, YFP+ cells were abundant at the lesion epicenter and a subset of the YFP+ cells demonstrated typical Schwann cell markers and morphology in the dorsal columns (***c'***, ***c''***) and in close proximity to a cavitation at the epicenter (***d***, ***d'***). All images were taken in spinal cord cross sections. Scale bars: ***a–c***, 200 μm; ***d***, 50 μm; ***a'***, 20 μm; ***b'***, ***b''***, ***b'''***, ***c'***, ***c''***, ***d'***, 10 μm.

weeks after SCI were derived from PDGFRα cells and their progeny. Keeping in mind that PDGFRα labels several populations of cells in the spinal cord and dorsal root, these data are consistent with an early appearance of Schwann cells derived from PDGFRα^{NEG}cells, presumably migratory Schwann cells (see section below on peripheral derived Schwann cells and their contribution to injury), from the dorsal root entry zone coupled with an ongoing increase of Schwann cells derived from PDGFRα+ cells and their progeny.

Olig2+ cells give rise to P0+ Schwann cells in response to contusion SCI

Considering that fate mapping using *PDGFR-αCreER:-YFP* or *-mGFP* mice labels other cell types in addition to OPCs, we wanted to test whether cells specific to the oligodendroglial lineage can give rise to P0+ myelinating Schwann cells after SCI. We lineage traced the Olig2+ cells using *Olig2-CreER:YFP* mice. In the spinal cord of uninjured control *Olig2-CreER:YFP* mice, we observed tamoxifen-induced recombination in oligodendrocytes and OPCs (Fig. 7*a*), as well as in a subset of gray matter astrocytes, as previously described (Dimou et al., 2008). Importantly, unlike the *PDGFRα-CreER:-YFP* or *-mGFP* lines, there was no recombination in vascular-associated cells, central canal-associated cells, or cells in the dorsal roots (Fig. 7*b*), suggesting that the only cellular overlap between *Olig2-CreER* and *PDGFRα-CreER* is with OPCs. Despite having a low recombination efficiency in OPCs at time of injury compared with the *PDGFRα CreER* mice, *Olig2CreER:YFP*+ cells were encountered in the dorsal columns (Fig. 7*c*) and adjacent to the lesion epicenter cavity, at 12 weeks after SCI (Fig. 7*d*). A subset of these recombined cells expressed P0 and exhibited the morphology of typical myelinating Schwann cells (Fig. 7*d*). This confirms that cells of the oligodendroglial lineage give rise to myelinating Schwann cells after contusion SCI.

Recombined PDGFRα-expressing cells from the PNS do not give rise to myelinating Schwann cells *in vitro* or *in vivo*

Migration of Schwann cells from the periphery into the CNS parenchyma was originally considered the primary source of myelinating Schwann cells after SCI (Franklin and Blakemore, 1993). To examine the potential of peripheral PDGFRα-expressing cells to give rise to myelinating Schwann cells, we FACS-isolated GFP+ (and GFP^{NEG}) cells from

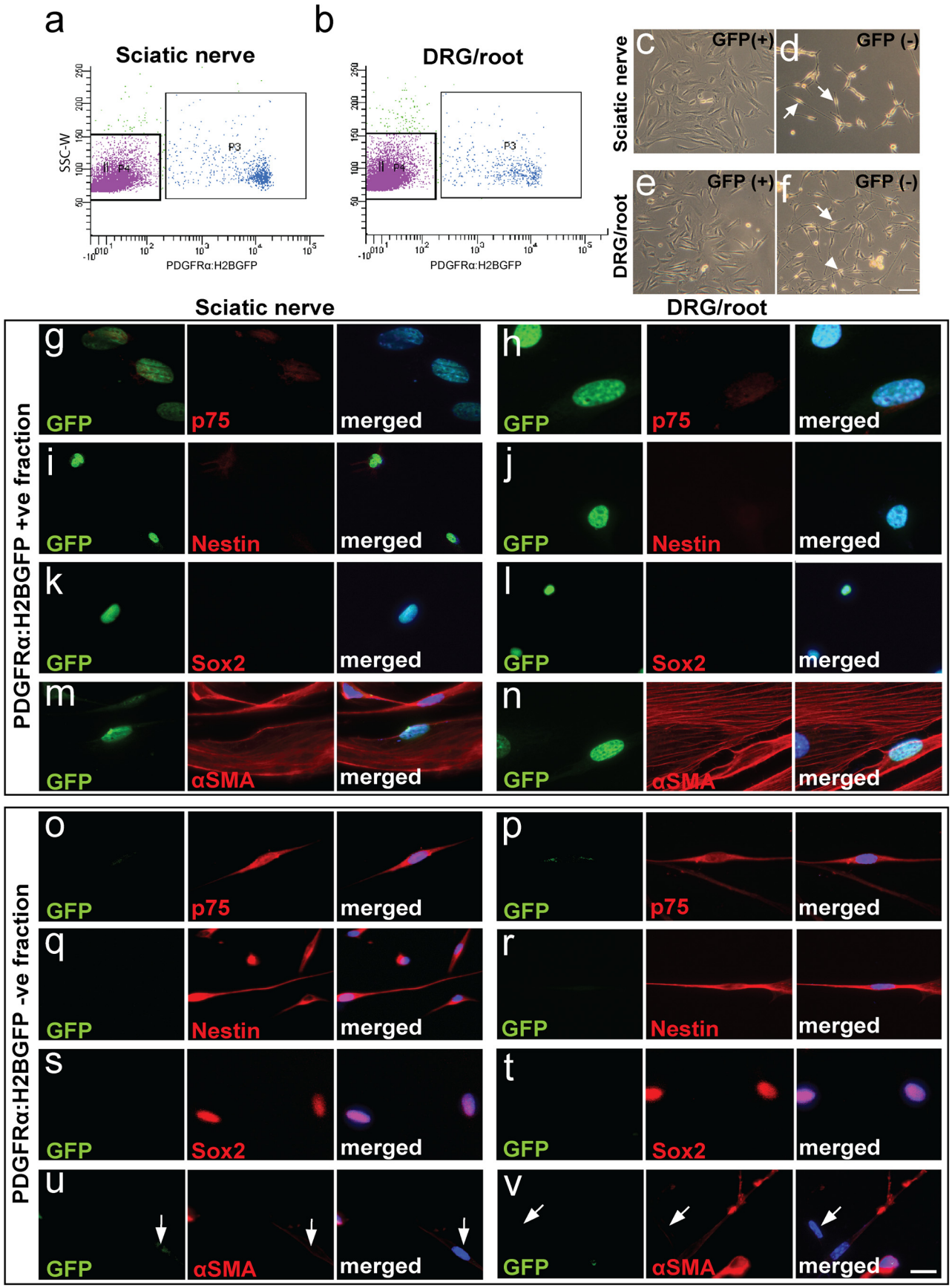

Figure 8. PDGFRα+ cells from the adult DRG and spinal root of *PDGFRα:H2BGFP* mice do not exhibit Schwann cell fate *in vitro*. Sciatic nerve (***a***) and DRG/spinal root (***b***) -derived cell suspensions from adult *PDGFRα:H2BGFP* mice were sorted for GFP-expression by FACS. ***c–f***, PDGFRα:H2BGFP+ and PDGFRα:H2BGFP^{NEG} cells were grown in Schwann cell proliferation/differentiation media for 1 week. The bipolar morphology of PDGFRαH2BGFP^{NEG} cells was consistent with Schwann cell differentiation (***d***, ***f***, arrow). PDGFRαH2BGFP+ (*Figure legend continues.*)

dorsal root/DRG and from sciatic nerves of adult *PDGFRα:H2B-GFP* mice and characterized the fate of these cells *in vitro* (Fig. 8). When grown in Schwann cell proliferation/differentiation media for 1 week, GFP^{NEG} cells exhibited a bipolar morphology consistent with Schwann cell differentiation (Fig. 8*d*,*f*), whereas GFP+ cells assumed a flattened morphology (Fig. 8*c*,*e*). Cells from the GFP^{NEG} cell fraction (Fig. 6*o–v*) expressed proteins characteristic of Schwann cell precursors, such as p75 (*o*,*p*), nestin (*q*,*r*), and Sox2 (*s*,*t*). In contrast, GFP+ cells (Fig. 8*g–n*) did not express Schwann cell lineage markers, but expressed αSMA, consistent with a fibroblast-like fate.

Considering that progenitor populations can behave differently in their quiescent state compared with in the wake of injury, where they have been noted to proliferate and contribute to repair (Joe et al., 2010; Almad et al., 2011), we wanted to specifically look at the responses of the peripheral PDGFRα recombined precursors in response to local injury. To determine whether injury-activated PDGFRα+ cells in the dorsal root or sciatic nerve produce myelinating Schwann cells, *PDFGRα-CreER: mGFP* mice were given tamoxifen 2 weeks before dorsal root (Fig. 9*a*,*b*,*d*) and sciatic nerve (Fig. 9*c*) crush injuries. After PNS injury, recombined cells with a flattened and branched morphology were numerous in the endoneurial spaces (Figure 9*a–c*). Twelve weeks after dorsal root crush (Fig. 9*d*), there was no evidence of mGFP+/P0+ Schwann cells in the dorsal root (Fig. 9*d*′,*d*″) or DRG (Fig. 9*d*‴). In the PNS, neither dorsal root injury nor sciatic nerve crush stimulated PDGFRα cells to express the Schwann cell marker P0; PDGFRα derived cells also did not possess Schwann cell morphology or close associations with axons (Fig. 9*a–d*). Consistent with these findings, inadvertent spinal cord damage during dorsal root injury did stimulate recombined cells to express P0, indicative of Schwann cell production, but these cells were restricted within the injured spinal cord (Fig. 9*d*, below dotted line). These findings indicate that PDGFRα-expressing cells residing in the PNS do not give rise to Schwann cells *in vitro* nor after local PNS injury *in vivo*.

Peripheral myelinating Schwann cells migrate into the spinal cord after injury and contribute to myelination

To examine the contribution of mature, myelinating Schwann cells in the PNS to myelination after SCI, we used *P0Cre-ER:YFP* mice. In uninjured control mice, recombination occurred in only 6.9 ± 1.18% and 24.1 ± 2.37% of the dorsal and ventral myelinating Schwann cells, respectively; no recombination was observed within the CNS (Fig. 10*a–d*), as expected from the specificity of P0 for PNS myelin. Twelve weeks after SCI, a small population of myelinating Schwann cells was observed at the lesion epicenter (Fig. 10*e*,*e*′). Importantly, the relative contribution of the recombined YFP+/P0+ myelin sheaths was small relative to the number of P0+ myelin sheaths both 3 and 12 weeks after SCI (Fig. 10*f*). When taking the low recombination efficacy into consideration, the percentage of P0+ cell-derived Schwann cells is <10% of the total P0+ tubes in the injured spinal cord, supporting the notion that OPCs generate the majority of Schwann cells in the cord after SCI.

Discussion

Here we determined which cell types contribute to the regeneration of myelin following contusion SCI, by systematically assessing the contributions of PDGFRα+, Olig2+, and P0+ cells to the generation of myelinating glia and axonal ensheathment/myelination following SCI.

The extent and source of spontaneous remyelination in the injured spinal cord has been the focus of considerable interest and debate, with important implications for treatment development after SCI. Previous fate mapping experiments of PDGFRα progeny using various recombination time points after SCI revealed that oligodendrogenesis and new myelin formation is an ongoing process in chronic SCI (Hesp et al., 2015). Here, we recombined PDGFRα cells before an injury to characterize the amount of *de novo* oligodendrocyte- and Schwann cell-derived myelination over time. At 12 weeks post-injury, we found extensive increases in new oligodendrocyte formation and in ensheathment/myelination by oligodendrocytes derived from PDGFRα+ progenitors labeled before injury. Importantly, the vast majority of myelinating Schwann cells in the injured spinal cord are centrally derived: both PDGFRα+ progenitors and Olig2-expressing cells gave rise to myelinating Schwann cells, whereas only a minority was derived from the P0+ peripheral population.

OPC derived ensheathment/myelination is substantial after SCI

The notion of ongoing demyelination after SCI as a pathological process limiting functional recovery (Blight, 1983; Totoiu and Keirstead, 2005) has fueled both preclinical and clinical research (Plemel et al., 2014). There is some evidence in preclinical work that transplanting myelinating cells can increase or accelerate myelin repair compared with spontaneous repair (Keirstead et al., 2005; Karimi-Abdolrezaee et al., 2006; Cao et al., 2010; All et al., 2015). Consistent with previous findings, we observed extensive oligodendrocyte production from OPCs in the astrocyte-rich parenchyma surrounding the injury (McTigue et al., 2001; Tripathi and McTigue, 2007; Sellers et al., 2009; Hesp et al., 2015) and the contribution of new oligodendrocytes to the myelination of axons in the chronic injury site (Hesp et al., 2015). By tracking cumulative myelination of spinal axons over time after injury (Fig. 4), we found that spontaneous myelination is progressive over time: at 3 weeks after SCI, *de novo* ensheathment/myelination accounted for ~15% of all MBP+ myelin sheaths, and by 12 weeks post-SCI this number approximated 30% at injury epicenter. Considering that the overall myelin (Fig. 4*c*) did not demonstrate a significant change between 3 and 12 wpi and yet there is a significant increase in the amount of new myelin (Fig. 4*d*), this suggests that myelin is being turned over and replaced between 3 and 12 wpi. To our surprise, approximately one-third of the 6000 *de novo* ensheathments did not reveal MBP expression at 12 wpi indicative of OPC processes or early oligodendrocyte ensheathments. Together, there is considerable new myelin production after SCI and even in the chronic setting there is ongoing myelin turnover.

These findings of extensive new myelin production after SCI may be an important contributor to functional recovery after SCI. Still, new myelin production may not just represent a regenerative process for the sole purpose of regenerating lost myelin segments. For example, even in the fully myelinated optic nerve

←

(*Figure legend continued.*) cells derived from both peripheral sources exhibited a flattened morphology under the same conditions. ***g–n***, Consistent with morphological findings, PDGFRαH2BGFP+ cells derived from the sciatic nerve (***g***, ***i***, ***k***, ***m***) or DRG/roots (***h***, ***j***, ***l***, ***n***) did not express Schwann cell lineage markers such as p75 (***g***, ***h***), nestin (***i***, ***j***), and Sox2 (***k***, ***l***) but expressed αSMA, consistent with a fibroblast-like phenotype. ***o–v***, In contrast, isolated PDGFRα:H2BGFP^{NEG} cells derived from the sciatic nerve (***o***, ***q***, ***s***, ***u***) or DRG/roots (***p***, ***r***, ***t***, ***v***) expressed markers of Schwann cell precursors such as p75 (***o***, ***p***), nestin (***q***, ***r***), and Sox2 (***s***, ***t***). Some αSMA^{NEG} cells were found in the GFP^{NEG} fraction (***u***, ***v***, arrows). Scale bars: ***c–f***, 100 μm; ***g–v***, 20 μm.

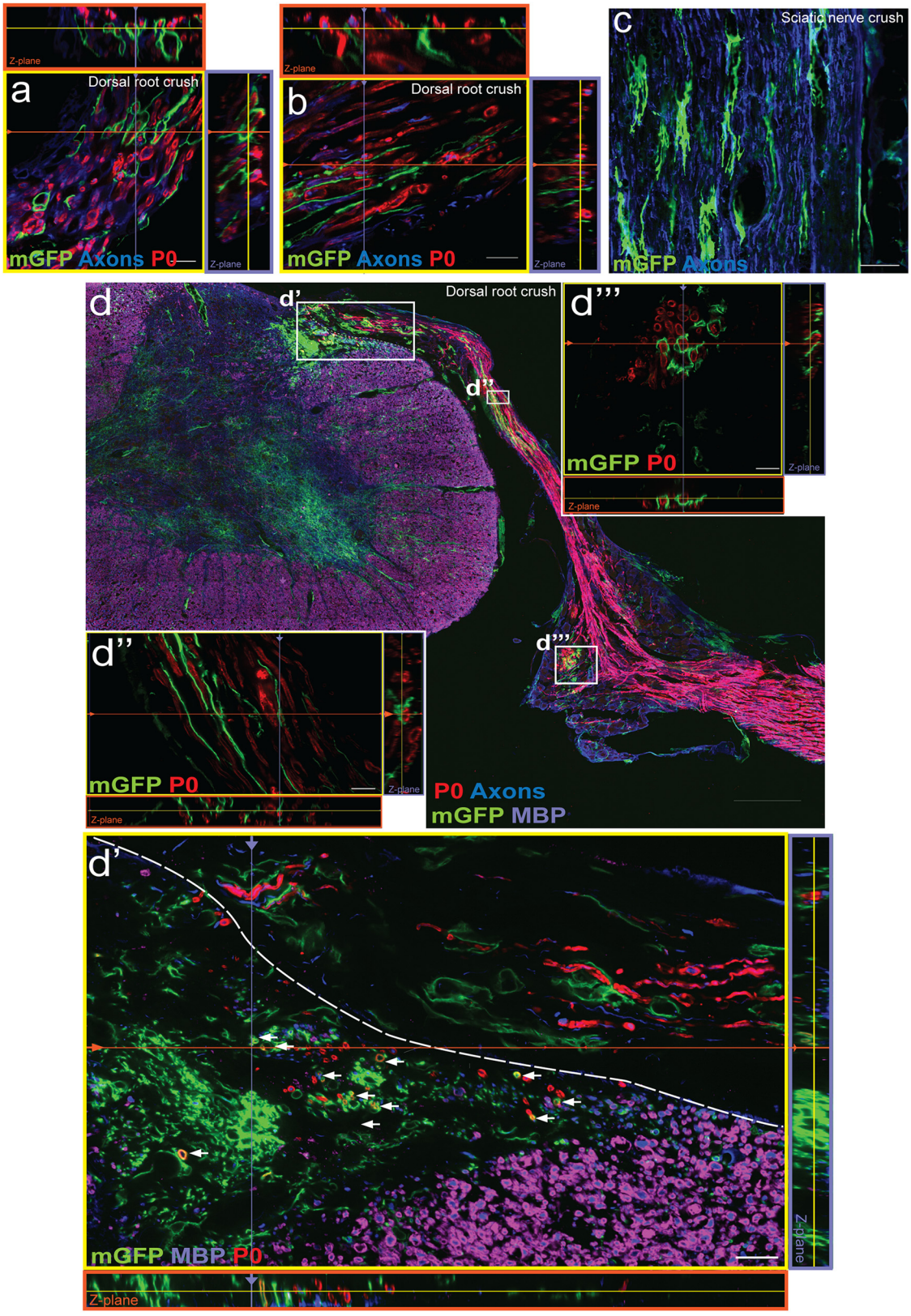

Figure 9. Recombined PDGFRα+ cells in the PNS do not give rise to P0+ cells in response to peripheral injury. ***a–c***, Four weeks after dorsal root crush (***a***, ***b***) or sciatic nerve crush injury in *PDGFRαCreER:mGFP* mice (***c***), mGFP+ cells had branched and flattened processes extending in the endoneurium between clusters of P0+ myelinating Schwann cells. Twelve weeks after a severe dorsal root crush injury (***d***), there was no evidence of mGFP+/P0+ Schwann cells in the dorsal root (***d′***, ***d″***) or the DRG (***d‴***). Only the injured spinal cord harbored recombined cells expressing both mGFP and P0. (***d′***, arrows). Images were taken in root or sciatic nerve longitudinal sections (***a–c***) or spinal cord cross sections (***d***). Scale bars: ***d***, 200 μm; ***d′***, 50 μm; ***d‴***, 20 μm; ***a–d″***, 10 μm.

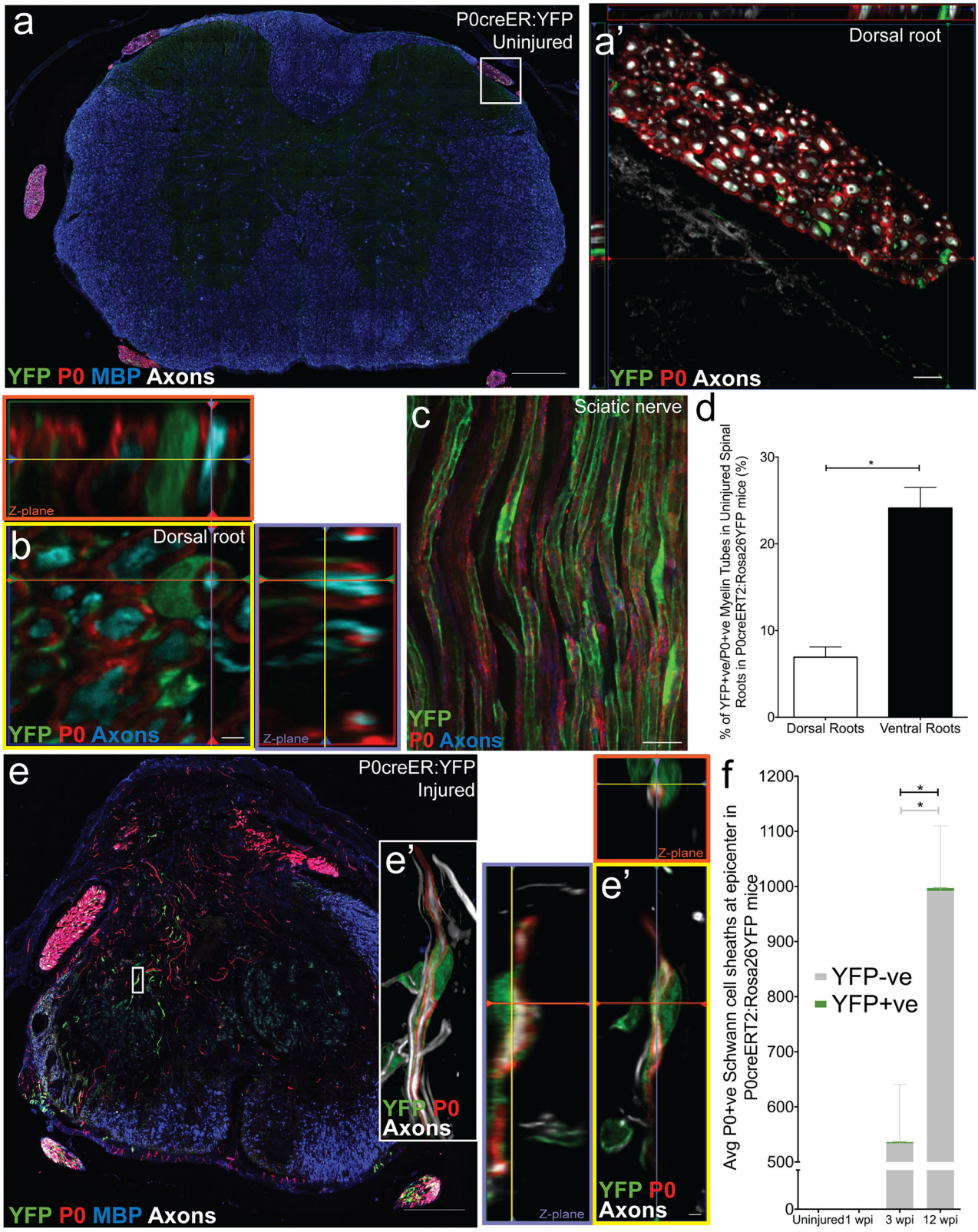

Figure 10. P0+ Schwann cells give rise to a small number of P0+ Schwann cells after SCI. In uninjured controls, no recombination was observed within the thoracic spinal cord *P0creER:YFP* mice (***a***); recombination (YFP; green) was only observed in the PNS surrounding P0+ tubes consistent with Schwann cell morphology (dorsal root: ***a'***; sciatic nerve: ***c***). Assessment of recombination efficiency in the uninjured roots revealed more YFP+ (green) P0+ (red) tubes in the ventral roots compared with the dorsal roots (***d***). ***e***, ***f***, Twelve weeks after SCI, YFP+ myelinating Schwann cells were observed at the injury epicenter of *P0creERT2:YFP* mice treated with tamoxifen 2 weeks before injury (***e***, ***e'***). The relative contribution of YFP+/P0+ myelin sheaths was low relative to the total number of P0+ myelin sheaths at both 3 and 12 wpi (<5 Schwann cell sheaths per section). There were significantly more overall P0+ profiles (gray + green bar; $U_{(11)} = 7.00$, $p = 0.046$) and more P0+/YFP^{NEG} profiles (gray portion of bar; $U_{(11)} = 7.00$, $p = 0.046$) at 12 wpi compared with 3 wpi. Images were taken in spinal cord cross sections (***a***), dorsal root cross sections (***b***), sciatic nerve longitudinal sections (***c***), or spinal cord cross sections at epicenter (***e***). *$p < 0.05$. Scale bars: ***a***, ***e***, 200 μm; ***c***, 20 μm; a', 10 μm; ***b***, ***e'***, 2 μm. Error bars represent the SEM.

and in the absence of demyelination there is *de novo* myelination by intercalation between existing myelin sheaths (Young et al., 2013). Such *de novo* myelination that is not linked with active or ongoing demyelination may occur after SCI, and is unlikely to contribute to functional recovery. Even if new myelin production is regenerative (i.e., replacing lost myelin), we cannot differentiate between ensheathment/myelination of spared axons, proximal stumps of cut axons that have been severed outside of the plane of section, or newly sprouted axons. This is important because we do not yet know whether newly ensheathed/myelinated axons are functional. Oligodendrocytes can myelinate even dead axons and/or artificial axons (Lee et al., 2012, 2013; Bechler et al., 2015) and thus some of the new myelin produced after SCI might be around severed axons, which is unlikely to provide a functional benefit. These considerations underscore the importance of addressing the functional importance of new myelin production and how it is associated with spontaneous recovery after SCI.

The majority of myelinating Schwann cells in the contused spinal cord are derived from PDGFRα+ CNS progenitors

For many decades and in diverse animal models, Schwann cells have been observed in the injured spinal cord, including in humans (M. B. Bunge et al., 1961; Bresnahan, 1978; R. P. Bunge et al., 1993; Beattie et al., 1997; Guest et al., 2005; James et al., 2011). Schwann cells are generally believed to migrate in from the PNS to contribute to myelination within the CNS (Franklin and Blakemore, 1993; Sims et al., 1998; Jasmin et al., 2000). Here, we demonstrate that ~70–80% of the myelinating Schwann cell profiles in the spinal cord 12 weeks post-contusion SCI are derived from resident PDGFRα+ cells. The CNS origin of Schwann cells is supported by our findings that Olig2-recombined cells also give rise to myelinating Schwann cells after SCI. We conclude that PDGFRα+ OPCs thus are the primary contributor to the myelinating Schwann cell population observed in the injured spinal cord. We also estimate that <10% of the myelinating Schwann cell profiles in the cord after injury are derived from peripheral myelinating Schwann cells. Therefore, via these indirect measurements, we can only account for the cellular origin of ~80–90% of the myelinating Schwann cells encountered in the contused spinal cord suggesting the existence of one or more other contributing cell populations. It is possible that non-myelinating Schwann cells or other DRG progenitors (Vidal et al., 2015) could be producing Schwann cells in response to injury.

The generation of Schwann cells from PDGFRα+ OPCs after CNS injury, and not from migration and/or differentiation of recombined PDGFRα+ precursors residing in the dorsal or ventral roots, is consistent with previous observations after focal chemical demyelination of the spinal cord (Zawadzka et al., 2010). In agreement, OPCs transplanted into demyelination lesions are able to generate Schwann cells (Talbott et al., 2005, 2006). A recent study proposed a CNS origin of Schwann cells after SCI on the basis of dorsal rhizotomies (Bartus et al., 2016). Here we provide conclusive evidence using fate mapping of various candidate cells expressing Cre from the PDGFRα and Olig2 promoters after contusion injury. The production of Schwann cells from OPCs is not observed in culture or after cotransplantation with astrocytes and thus differentiation is BMP-dependent (Talbott et al., 2006). Monteiro de Castro et al. (2015) recently reported that cell-specific deletion of STAT3 in astrocytes decreases remyelination by oligodendrocytes in favor of Schwann cells using a chemical demyelination model. Together, these findings suggest that an astrocyte-derived signal is required for OPC differentiation into oligodendrocytes. In agreement with this hypothesis, OPC-derived Schwann cell differentiation was observed after contusion SCI mainly in the dorsal columns where astrocytes are rare. Astrocytes within these regions may also be phenotypically different from astrocytes in other regions of the cord (Tsai et al., 2012). A better understanding of the regenerative potential of OPCs and their molecular regulation may provide new avenues in CNS repair.

Schwann cell transplantation elicits moderate functional improvements in preclinical models (Pearse et al., 2004; Biernaskie et al., 2007; Sparling et al., 2015) and is currently being studied in clinical trials (Clinical trial.gov: NCT01739023, NCT0235425). Schwann cell transplantation can result in an even greater endogenous Schwann cell response after SCI (Hill et al., 2006; Biernaskie et al., 2007; Sparling et al., 2015). Therefore, gaining a better understanding of the endogenous Schwann cell response observed after injury in both rodents and humans could help to develop future treatment strategies. Importantly, the finding of Schwannosis in the chronic clinically injured SCI population (Bruce et al., 2000; Norenberg et al., 2004) has been discussed as a cause of functional decline pointing to the need for a better understanding the biological processes regulating Schwann cell production after SCI. Transgenic deletion of neuregulin-1 in all cells prevented myelination by Schwann cells in the injured spinal cord of mice and these mice showed worse functional outcomes in an open field locomotor test as early as 1 week after SCI (Bartus et al., 2016). However, this recovery could also be due to other neuroprotective effects of neuregulin-1 after SCI (Gauthier et al., 2013; Alizadeh et al., 2017). Hence, the functional significance of endogenous Schwann cell myelination still remains to be shown. This formation of Schwann cells in the areas of most extensive spinal cord damage, where astrocytes become sparse, might represent an endogenous repair mechanism and a target for future therapeutic interventions; bridging severe injuries by stimulating OPCs to produce Schwann cells might allow for a more conducive environment for axonal growth and myelin formation.

Conclusion

Endogenous OPCs are capable of extensive myelination after SCI. The majority of OPCs remains lineage-restricted and produces myelinating oligodendrocytes that ensheath axons. PDGFRα+ cells (likely OPCs) are the source of the majority of Schwann cells present in the spinal cord after clinically relevant (contusion) SCI. This repair mechanism by endogenous, CNS-derived Schwann cells may represent a novel therapeutic target for repairing the injured spinal cord in areas of grossly disrupted cytoarchitecture.

References

Alizadeh A, Dyck SM, Kataria H, Shahriary GM, Nguyen DH, Santhosh KT, Karimi-Abdolrezaee S (2017) Neuregulin-1 positively modulates glial response and improves neurological recovery following traumatic spinal cord injury. Glia 65:1152–1175. CrossRef Medline

All AH, Gharibani P, Gupta S, Bazley FA, Pashai N, Chou BK, Shah S, Resar LM, Cheng L, Gearhart JD, Kerr CL (2015) Early intervention for spinal cord injury with human induced pluripotent stem cells oligodendrocyte progenitors. PLoS One 10:e0116933. CrossRef Medline

Almad A, Sahinkaya FR, McTigue DM (2011) Oligodendrocyte fate after spinal cord injury. Neurotherapeutics 8:262–273. CrossRef Medline

Assinck P, Duncan GJ, Hilton BJ, Plemel JR, Tetzlaff W (2017) Cell transplantation therapy for spinal cord injury. Nat Neurosci 20:637–647. CrossRef Medline

Barnabé-Heider F, Göritz C, Sabelström H, Takebayashi H, Pfrieger FW, Meletis K, Frisén J (2010) Origin of new glial cells in intact and injured adult spinal cord. Cell Stem Cell 7:470–482. CrossRef Medline

Bartus K, Galino J, James ND, Hernandez-Miranda LR, Dawes JM, Fricker FR, Garratt AN, McMahon SB, Ramer MS, Birchmeier C, Bennett DL,

Bradbury EJ (2016) Neuregulin-1 controls an endogenous repair mechanism after spinal cord injury. Brain 139:1394–1416. CrossRef Medline
Beattie MS, Bresnahan JC, Komon J, Tovar CA, Van Meter M, Anderson DK, Faden AI, Hsu CY, Noble LJ, Salzman S, Young W (1997) Endogenous repair after spinal cord contusion injuries in the rat. Exp Neurol 148:453–463. CrossRef Medline
Bechler ME, Byrne L, Ffrench-Constant C (2015) CNS myelin sheath lengths are an intrinsic property of oligodendrocytes. Curr Biol 25:2411–2416. CrossRef Medline
Biernaskie J, Sparling JS, Liu J, Shannon CP, Plemel JR, Xie Y, Miller FD, Tetzlaff W (2007) Skin-derived precursors generate myelinating Schwann cells that promote remyelination and functional recovery after contusion spinal cord injury. J Neurosci 27:9545–9559. CrossRef Medline
Blakemore WF (1974) Pattern of remyelination in the CNS. Nature 249:577–578. CrossRef Medline
Blakemore WF (1975) Remyelination by Schwann cells of axons demyelinated by intraspinal injection of 6-aminonicotinamide in the rat. J Neurocytol 4:745–757. CrossRef Medline
Blight AR (1983) Cellular morphology of chronic spinal cord injury in the cat: analysis of myelinated axons by line-sampling. Neuroscience 10:521–543. CrossRef Medline
Bresnahan JC (1978) An electron-microscopic analysis of axonal alterations following blunt contusion of the spinal cord of the rhesus monkey (*Macaca mulatta*). J Neurol Sci 37:59–82. CrossRef Medline
Bresnahan JC, King JS, Martin GF, Yashon D (1976) A neuroanatomical analysis of spinal cord injury in the rhesus monkey (*Macaca mulatta*). J Neurol Sci 28:521–542. CrossRef Medline
Bruce JH, Norenberg MD, Kraydieh S, Puckett W, Marcillo A, Dietrich D (2000) Schwannosis: role of gliosis and proteoglycan in human spinal cord injury. J Neurotrauma 17:781–788. CrossRef Medline
Bujalka H, Koenning M, Jackson S, Perreau VM, Pope B, Hay CM, Mitew S, Hill AF, Lu QR, Wegner M, Srinivasan R, Svaren J, Willingham M, Barres BA, Emery B (2013) MYRF is a membrane-associated transcription factor that autoproteolytically cleaves to directly activate myelin genes. PLoS Biol 11:e1001625. CrossRef Medline
Bunge MB, Bunge RP, Ris H (1961) Ultrastructural study of remyelination in an experimental lesion in adult cat spinal cord. J Biophys Biochem Cytol 10:67–94. CrossRef Medline
Bunge RP, Bunge MB, Rish (1960) Electron microscopic study of demyelination in an experimentally induced lesion in adult cat spinal cord. J Biophys Biochem Cytol 7:685–696. CrossRef Medline
Bunge RP, Puckett WR, Becerra JL, Marcillo A, Quencer RM (1993) Observations on the pathology of human spinal cord injury: a review and classification of 22 new cases with details from a case of chronic cord compression with extensive focal demyelination. Adv Neurol 59:75–89. Medline
Cao Q, He Q, Wang Y, Cheng X, Howard RM, Zhang Y, DeVries WH, Shields CB, Magnuson DS, Xu XM, Kim DH, Whittemore SR (2010) Transplantation of ciliary neurotrophic factor-expressing adult oligodendrocyte precursor cells promotes remyelination and functional recovery after spinal cord injury. J Neurosci 30:2989–3001. CrossRef Medline
Crowe MJ, Bresnahan JC, Shuman SL, Masters JN, Beattie MS (1997) Apoptosis and delayed degeneration after spinal cord injury in rats and monkeys. Nat Med 3:73–76. CrossRef Medline
Cummings BJ, Uchida N, Tamaki SJ, Salazar DL, Hooshmand M, Summers R, Gage FH, Anderson AJ (2005) Human neural stem cells differentiate and promote locomotor recovery in spinal cord-injured mice. Proc Natl Acad Sci U S A 102:14069–14074. CrossRef Medline
Dimou L, Simon C, Kirchhoff F, Takebayashi H, Götz M (2008) Progeny of Olig2-expressing progenitors in the gray and white matter of the adult mouse cerebral cortex. J Neurosci 28:10434–10442. CrossRef Medline
Emery B, Agalliu D, Cahoy JD, Watkins TA, Dugas JC, Mulinyawe SB, Ibrahim A, Ligon KL, Rowitch DH, Barres BA (2009) Myelin gene regulatory factor is a critical transcriptional regulator required for CNS myelination. Cell 138:172–185. CrossRef Medline
Franklin RJ, Blakemore WF (1993) Requirements for Schwann cell migration within CNS environments: a viewpoint. Int J Dev Neurosci 11:641–649. CrossRef Medline
Gauthier MK, Kosciuczyk K, Tapley L, Karimi-Abdolrezaee S (2013) Dysregulation of the neuregulin-1-ErbB network modulates endogenous oligodendrocyte differentiation and preservation after spinal cord injury. Eur J Neurosci 38:2693–2715. CrossRef Medline
Göritz C, Dias DO, Tomilin N, Barbacid M, Shupliakov O, Frisén J (2011) A pericyte origin of spinal cord scar tissue. Science 333:238–242. CrossRef Medline
Grégoire CA, Goldenstein BL, Floriddia EM, Barnabé-Heider F, Fernandes KJ (2015) Endogenous neural stem cell responses to stroke and spinal cord injury. Glia 63:1469–1482. CrossRef Medline
Guest JD, Hiester ED, Bunge RP (2005) Demyelination and Schwann cell responses adjacent to injury epicenter cavities following chronic human spinal cord injury. Exp Neurol 192:384–393. CrossRef Medline
Hamilton TG, Klinghoffer RA, Corrin PD, Soriano P (2003) Evolutionary divergence of platelet-derived growth factor alpha receptor signaling mechanisms. Mol Cell Biol 23:4013–4025. CrossRef Medline
Hesp ZC, Goldstein EZ, Miranda CJ, Kaspar BK, McTigue DM (2015) Chronic oligodendrogenesis and remyelination after spinal cord injury in mice and rats. J Neurosci 35:1274–1290. CrossRef Medline
Hill CE, Moon LD, Wood PM, Bunge MB (2006) Labeled Schwann cell transplantation: cell loss, host Schwann cell replacement, and strategies to enhance survival. Glia 53:338–343. CrossRef Medline
Itoyama Y, Ohnishi A, Tateishi J, Kuroiwa Y, Webster HD (1985) Spinal cord multiple sclerosis lesions in Japanese patients: Schwann cell remyelination occurs in areas that lack glial fibrillary acidic protein (GFAP). Acta Neuropathol 65:217–223. CrossRef Medline
James ND, Bartus K, Grist J, Bennett DL, McMahon SB, Bradbury EJ (2011) Conduction failure following spinal cord injury: functional and anatomical changes from acute to chronic stages. J Neurosci 31:18543–18555. CrossRef Medline
Jasmin L, Janni G, Moallem TM, Lappi DA, Ohara PT (2000) Schwann cells are removed from the spinal cord after effecting recovery from paraplegia. J Neurosci 20:9215–9223. Medline
Joe AW, Yi L, Natarajan A, Le Grand F, So L, Wang J, Rudnicki MA, Rossi FM (2010) Muscle injury activates resident fibro/adipogenic progenitors that facilitate myogenesis. Nat Cell Biol 12:153–163. CrossRef Medline
Kang SH, Fukaya M, Yang JK, Rothstein JD, Bergles DE (2010) NG2+ CNS glial progenitors remain committed to the oligodendrocyte lineage in postnatal life and following neurodegeneration. Neuron 68:668–681. CrossRef Medline
Karimi-Abdolrezaee S, Eftekharpour E, Wang J, Morshead CM, Fehlings MG (2006) Delayed transplantation of adult neural precursor cells promotes remyelination and functional neurological recovery after spinal cord injury. J Neurosci 26:3377–3389. CrossRef Medline
Keirstead HS, Nistor G, Bernal G, Totoiu M, Cloutier F, Sharp K, Steward O (2005) Human embryonic stem cell-derived oligodendrocyte progenitor cell transplants remyelinate and restore locomotion after spinal cord injury. J Neurosci 25:4694–4705. CrossRef Medline
Kitada M, Rowitch DH (2006) Transcription factor co-expression patterns indicate heterogeneity of oligodendroglial subpopulations in adult spinal cord. Glia 54:35–46. CrossRef Medline
Koenning M, Jackson S, Hay CM, Faux C, Kilpatrick TJ, Willingham M, Emery B (2012) Myelin gene regulatory factor is required for maintenance of myelin and mature oligodendrocyte identity in the adult CNS. J Neurosci 32:12528–12542. CrossRef Medline
Kwon BK, Oxland TR, Tetzlaff W (2002) Animal models used in spinal cord regeneration research. Spine 27:1504–1510. CrossRef Medline
Kwon BK, Tetzlaff W, Grauer JN, Beiner J, Vaccaro AR (2004) Pathophysiology and pharmacologic treatment of acute spinal cord injury. Spine J 4:451–464. CrossRef Medline
Lasiene J, Shupe L, Perlmutter S, Horner P (2008) No evidence for chronic demyelination in spared axons after spinal cord injury in a mouse. J Neurosci 28:3887–3896. CrossRef Medline
Lee S, Leach MK, Redmond SA, Chong SY, Mellon SH, Tuck SJ, Feng ZQ, Corey JM, Chan JR (2012) A culture system to study oligodendrocyte myelination processes using engineered nanofibers. Nat Methods 9:917–922. CrossRef Medline
Lee S, Chong SY, Tuck SJ, Corey JM, Chan JR (2013) A rapid and reproducible assay for modeling myelination by oligodendrocytes using engineered nanofibers. Nat Protoc 8:771–782. CrossRef Medline
Leone DP, Genoud S, Atanasoski S, Grausenburger R, Berger P, Metzger D, Macklin WB, Chambon P, Suter U (2003) Tamoxifen-inducible glia-specific Cre mice for somatic mutagenesis in oligodendrocytes and Schwann cells. Mol Cell Neurosci 22:430–440. CrossRef Medline
McTigue DM, Tripathi RB (2008) The life, death, and replacement of oligodendrocytes in the adult CNS. J Neurochem 107:1–19. CrossRef Medline

McTigue DM, Wei P, Stokes BT (2001) Proliferation of NG2-positive cells and altered oligodendrocyte numbers in the contused rat spinal cord. J Neurosci 21:3392–3400. Medline

Monteiro de Castro G, Deja NA, Ma D, Zhao C, Franklin RJ (2015) Astrocyte activation via Stat3 signaling determines the balance of oligodendrocyte versus Schwann cell remyelination. Am J Pathol 185:2431–2440. CrossRef Medline

Nishiyama A, Lin XH, Giese N, Heldin CH, Stallcup WB (1996) Co-localization of NG2 proteoglycan and PDGF alpha-receptor on O2A progenitor cells in the developing rat brain. J Neurosci Res 43:299–314. CrossRef Medline

Norenberg MD, Smith J, Marcillo A (2004) The pathology of human spinal cord injury: defining the problems. J Neurotrauma 21:429–440. CrossRef Medline

Pearse DD, Pereira FC, Marcillo AE, Bates ML, Berrocal YA, Filbin MT, Bunge MB (2004) cAMP and Schwann cells promote axonal growth and functional recovery after spinal cord injury. Nat Med 10:610–616. CrossRef Medline

Plemel JR, Keough MB, Duncan GJ, Sparling JS, Yong VW, Stys PK, Tetzlaff W (2014) Remyelination after spinal cord injury: is it a target for repair? Prog Neurobiol 117:54–72. CrossRef Medline

Powers BE, Lasiene J, Plemel JR, Shupe L, Perlmutter SI, Tetzlaff W, Horner PJ (2012) Axonal thinning and extensive remyelination without chronic demyelination in spinal injured rats. J Neurosci 32:5120–5125. CrossRef Medline

Powers BE, Sellers DL, Lovelett EA, Cheung W, Aalami SP, Zapertov N, Maris DO, Horner PJ (2013) Remyelination reporter reveals prolonged refinement of spontaneously regenerated myelin. Proc Natl Acad Sci U S A 110:4075–4080. CrossRef Medline

Priest CA, Manley NC, Denham J, Wirth ED 3rd, Lebkowski JS (2015) Preclinical safety of human embryonic stem cell-derived oligodendrocyte progenitors supporting clinical trials in spinal cord injury. Regen Med 10:939–958. CrossRef Medline

Rivers LE, Young KM, Rizzi M, Jamen F, Psachoulia K, Wade A, Kessaris N, Richardson WD (2008) PDGFRA/NG2 glia generate myelinating oligodendrocytes and piriform projection neurons in adult mice. Nat Neurosci 11:1392–1401. CrossRef Medline

Sellers DL, Maris DO, Horner PJ (2009) Postinjury niches induce temporal shifts in progenitor fates to direct lesion repair after spinal cord injury. J Neurosci 29:6722–6733. CrossRef Medline

Sims TJ, Durgun MB, Gilmore SA (1998) Schwann cell invasion of ventral spinal cord: the effect of irradiation on astrocyte barriers. J Neuropathol Exp Neurol 57:866–873. CrossRef Medline

Sparling JS, Bretzner F, Biernaskie J, Assinck P, Jiang Y, Arisato H, Plunet WT, Borisoff J, Liu J, Miller FD, Tetzlaff W (2015) Schwann cells generated from neonatal skin-derived precursors or neonatal peripheral nerve improve functional recovery after acute transplantation into the partially injured cervical spinal cord of the rat. J Neurosci 35:6714–6730. CrossRef Medline

Stenudd M, Sabelström H, Frisén J (2015) Role of endogenous neural stem cells in spinal cord injury and repair. JAMA Neurol 72:235–237. CrossRef Medline

Takebayashi H, Nabeshima Y, Yoshida S, Chisaka O, Ikenaka K, Nabeshima Y (2002) The basic helix-loop-helix factor olig2 is essential for the development of motoneuron and oligodendrocyte lineages. Curr Biol 12:1157–1163. CrossRef Medline

Talbott JF, Loy DN, Liu Y, Qiu MS, Bunge MB, Rao MS, Whittemore SR (2005) Endogenous Nkx2.2+/Olig2+ oligodendrocyte precursor cells fail to remyelinate the demyelinated adult rat spinal cord in the absence of astrocytes. Exp Neurol 192:11–24. CrossRef Medline

Talbott JF, Cao Q, Enzmann GU, Benton RL, Achim V, Cheng XX, Mills MD, Rao MS, Whittemore SR (2006) Schwann cell-like differentiation by adult oligodendrocyte precursor cells following engraftment into the demyelinated spinal cord is BMP-dependent. Glia 54:147–159. CrossRef Medline

Totoiu MO, Keirstead HS (2005) Spinal cord injury is accompanied by chronic progressive demyelination. J Comp Neurol 486:373–383. CrossRef Medline

Tripathi R, McTigue DM (2007) Prominent oligodendrocyte genesis along the border of spinal contusion lesions. Glia 55:698–711. CrossRef Medline

Tsai HH, Li H, Fuentealba LC, Molofsky AV, Taveira-Marques R, Zhuang H, Tenney A, Murnen AT, Fancy SP, Merkle F, Kessaris N, Alvarez-Buylla A, Richardson WD, Rowitch DH (2012) Regional astrocyte allocation regulates CNS synaptogenesis and repair. Science 337:358–362. CrossRef Medline

Vidal M, Maniglier M, Deboux C, Bachelin C, Zujovic V, Baron-Van Evercooren A (2015) Adult DRG stem/progenitor cells generate pericytes in the presence of central nervous system (CNS) developmental cues, and Schwann cells in response to CNS demyelination. Stem Cells 33:2011–2024. CrossRef Medline

Young KM, Psachoulia K, Tripathi RB, Dunn SJ, Cossell L, Attwell D, Tohyama K, Richardson WD (2013) Oligodendrocyte dynamics in the healthy adult CNS: evidence for myelin remodeling. Neuron 77:873–885. CrossRef Medline

Zawadzka M, Rivers LE, Fancy SP, Zhao C, Tripathi R, Jamen F, Young K, Goncharevich A, Pohl H, Rizzi M, Rowitch DH, Kessaris N, Suter U, Richardson WD, Franklin RJ (2010) CNS-resident glial progenitor/stem cells produce Schwann cells as well as oligodendrocytes during repair of CNS demyelination. Cell Stem Cell 6:578–590. CrossRef Medline